#### **GPCR SIGNALING**

# G protein–coupled receptor endocytosis generates spatiotemporal bias in $\beta$ -arrestin signaling

András D. Tóth<sup>1,2,3</sup>†, Bence Szalai<sup>1,2</sup>†‡, Orsolya T. Kovács<sup>2</sup>, Dániel Garger<sup>2,4</sup>, Susanne Prokop<sup>2</sup>, Eszter Soltész-Katona<sup>1</sup>, András Balla<sup>2,5</sup>, Asuka Inoue<sup>6</sup>, Péter Várnai<sup>2,5</sup>, Gábor Turu<sup>1,2</sup>\*, László Hunyady<sup>1,2</sup>\*

The stabilization of different active conformations of G protein–coupled receptors is thought to underlie the varying efficacies of biased and balanced agonists. Here, profiling the activation of signal transducers by angiotensin II type 1 receptor (AT\_1R) agonists revealed that the extent and kinetics of  $\beta$ -arrestin binding exhibited substantial ligand-dependent differences, which were lost when receptor internalization was inhibited. When AT\_1R endocytosis was prevented, even weak partial agonists of the  $\beta$ -arrestin pathway acted as full or near-full agonists, suggesting that receptor conformation did not exclusively determine  $\beta$ -arrestin recruitment. The ligand-dependent variance in  $\beta$ -arrestin translocation was much larger at endosomes than at the plasma membrane, showing that ligand efficacy in the  $\beta$ -arrestin pathway was spatiotemporally determined. Experimental investigations and mathematical modeling demonstrated how multiple factors concurrently shaped the effects of agonists on endosomal receptor– $\beta$ -arrestin binding and thus determined the extent of functional selectivity. Ligand dissociation rate and G protein activity had particularly strong, internalization-dependent effects on the receptor– $\beta$ -arrestin interaction. We also showed that endocytosis regulated the agonist efficacies of two other receptors with sustained  $\beta$ -arrestin binding: the V<sub>2</sub> vasopressin receptor and a mutant  $\beta$ <sub>2</sub>-adrenergic receptor. In the absence of endocytosis, the agonist-dependent variance in  $\beta$ -arrestin2 binding was markedly diminished. Our results suggest that endocytosis determines the spatiotemporal bias in GPCR signaling and can aid in the development of more efficacious, functionally selective compounds.



#### INTRODUCTION

G protein-coupled receptors (GPCRs) represent the largest family of cell surface receptors, and they engage various signaling proteins upon stimulation by their agonists. Certain ligands stimulate selective or stronger activation of different transducers, a phenomenon called biased signaling or functional selectivity (1). This concept has gained great attention because biased drugs may exert beneficial clinical effects because of their lack of engagement with signaling pathways that induce undesired side effects. Regarding biased signaling, the angiotensin II type 1 receptor (AT<sub>1</sub>R) is one of the most extensively studied GPCRs. Whereas its endogenous peptide ligand angiotensin II (AngII) serves as a full agonist for AT<sub>1</sub>R, several studies have shown that derivatives of AngII that lack an aromatic amino acid residue in the eighth position preferentially activate  $\beta$ -arrestin rather than G protein signaling (2, 3). Moreover, diverse functional actions of AT<sub>1</sub>R agonists have also been demonstrated across different G protein and GPCR kinase (GRK) subtypes (4-7). Furthermore, different ligand bias profiles have also been linked to specific in vivo effects,

<sup>1</sup>Institute of Molecular Life Sciences, Centre of Excellence of the Hungarian Academy of Sciences, HUN-REN Research Centre for Natural Sciences, Magyar tudósok körútja 2, H-1117 Budapest, Hungary. <sup>2</sup>Department of Physiology, Faculty of Medicine, Semmelweis University, Tűzoltó utca 37-47, H-1094 Budapest, Hungary. <sup>3</sup>Department of Internal Medicine and Haematology, Semmelweis University, Szentkirályi utca 46, H-1088 Budapest, Hungary. <sup>4</sup>Computational Health Center, Helmholtz Munich, Ingolstaedter Landstraße 1, 85764 Neuherberg, Germany. <sup>5</sup>HUN-REN-SE Laboratory of Molecular Physiology, Hungarian Research Network, Tűzoltó utca 37-47, H-1094 Budapest, Hungary. <sup>6</sup>Molecular and Cellular Biochemistry, Graduate School of Pharmaceutical Sciences, Tohoku University, 6-3, Aoba, Aramaki, Aoba-ku, Sendai, Miyagi, 980-8578 Japan.

and TRV120027, a  $\beta$ -arrestin-biased agonist of AT<sub>1</sub>R, has even been evaluated in clinical trials (8–12).

It was theorized that the pathway-selective cellular actions of biased ligands are based on their ability to stabilize receptors in different conformations (13, 14), which was later proven by the elucidation of corresponding crystal structures (15). Consistent with community guidelines, here we use the term "ligand bias" to refer to biased signaling emerging from distinct, agonist-induced receptor conformations (1). Despite having unique translational potential, it has remained elusive how ligand bias interferes with the generally known kinetic and spatial factors that regulate receptor signaling. Advancements in live cell-based sensors and genetically modified cell lines have greatly improved our understanding of how the temporal alteration or synchronization of signaling pathways can transmit specific information (16, 17). Moreover, the concept and importance of "temporal bias" is increasingly acknowledged, given that many studies have shown that the activities of distinct signaling pathways can differentially change over time, and the kinetics of these changes happen in a ligand-specific manner (1, 17–19). Furthermore, data suggest that some ligands exhibit "location bias" or "spatial bias," which means that they may differently stimulate receptor signaling in distinct subcellular compartments (20-23). These levels of complexity pose a great challenge to the precise experimental investigation of the kinetic and spatial factors that affect biased signaling and consequently complicate the rational design of novel pathway-selective clinical drugs.

Here, we aimed to identify the principal dynamic processes that act interdependently with ligand bias to evoke functionally selective cellular responses. To comprehensively investigate the spatiotemporal layer of biased signaling, we conducted a systematic series of advanced kinetic assays with a set of  $AT_1R$  agonists and formulated an in silico model of receptor signaling. We found that differences in the extent

<sup>\*</sup>Corresponding author. Email: turu.gabor@ttk.hun-ren.hu (G.T.); hunyady.laszlo@ttk.hun-ren.hu (L.H.)

<sup>†</sup>These authors contributed equally to this work.

<sup>‡</sup>Present address: Turbine Ltd., H-1027 Budapest, Bem József utca 9, Hungary.

of the interaction between AT<sub>1</sub>R and β-arrestin in response to distinct agonists, including balanced and biased ligands, were almost completely lost upon inhibition of receptor internalization, and the effects of the key regulatory factors that drive ligand specificity in β-arrestin binding were manifested at endosomes. Our results reveal a strong correlation between ligand dissociation rate and the extent of the  $AT_1R-\beta$ -arrestin interaction after receptor internalization. Furthermore, our experiments revealed that the recruitment of βarrestin2 to AT<sub>1</sub>R by balanced agonists was facilitated by the activity of members of the  $G_{q/11}$  family of G proteins, leading to the increased abundance of ÂT<sub>1</sub>R-β-arrestin complexes predominantly at the endosomal compartment. Last, our mathematical model and expanded experimental results with the V<sub>2</sub> vasopressin receptor  $(V_2R)$  and the  $\beta_2$ -adrenergic receptor ( $\beta_2AR$ ) suggest that endocytosis provides a general platform for kinetic and spatial factors to shape the overall signaling outcome together with ligand bias in a mutually dependent manner.

#### **RESULTS**

## Ligand-specific differences in AT<sub>1</sub>R-β-arrestin binding depend on receptor endocytosis

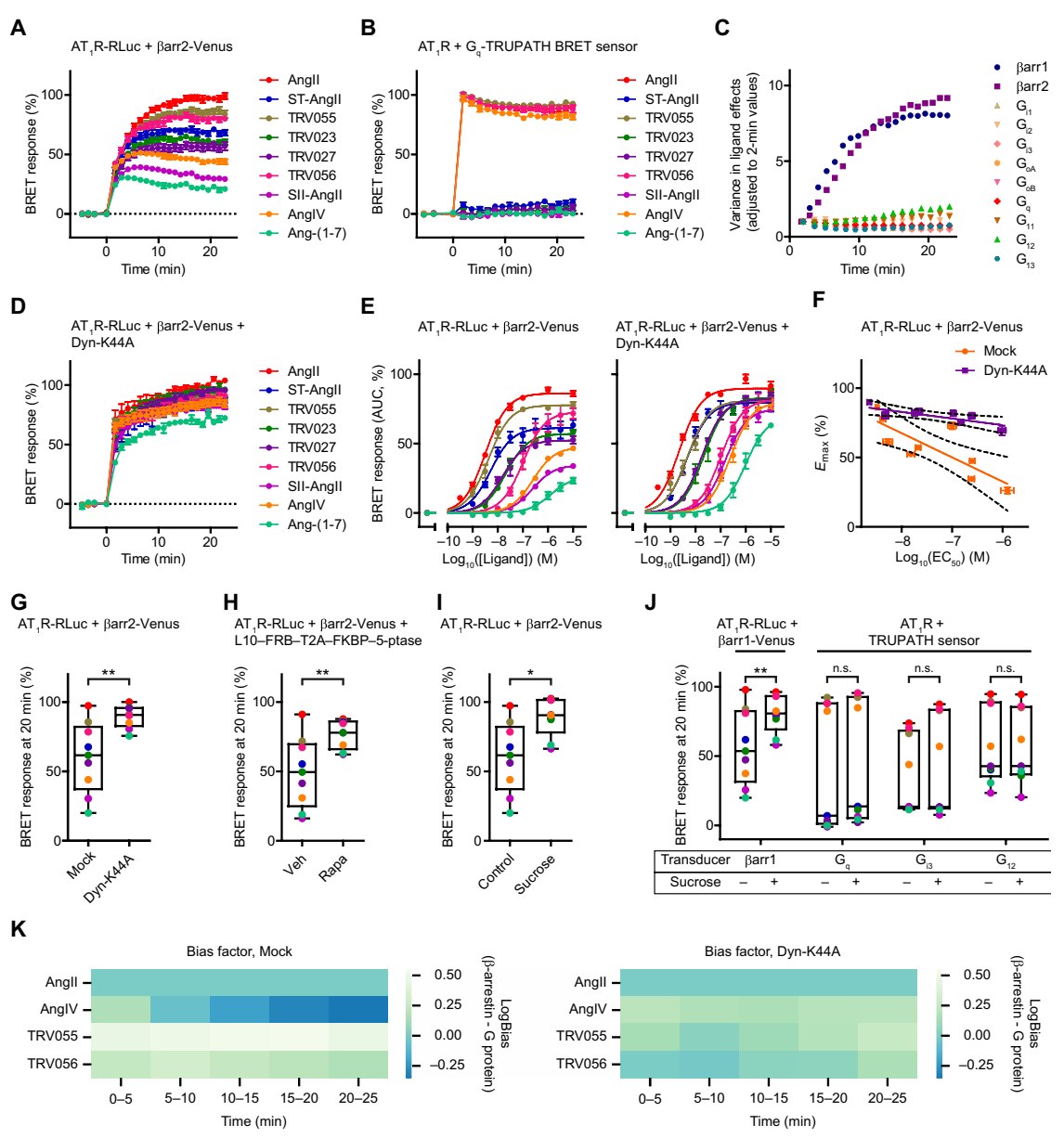
To comprehensively investigate the temporal characteristics of biased signaling, we monitored the activation of a large set of AT<sub>1</sub>R transducers in real time after stimulation with nine AT<sub>1</sub>R peptide ligands, which display markedly different affinities and signaling bias profiles (fig. S1) (24-26). All agonists were applied at a concentration of 10 µM, which results in complete or near-complete saturation of AT<sub>1</sub>R, and the endogenous agonist AngII was selected as the reference ligand. The receptor-β-arrestin interaction was assessed with a bioluminescence resonance energy transfer (BRET)based assay (27), whereby the BRET signal between RLuc-labeled  $AT_1R$  and Venus-tagged  $\beta$ -arrestin was measured. All of the ligands stimulated the binding of  $\beta$ -arrestin1 (fig. S2) and  $\beta$ -arrestin2 (Fig. 1A) to AT<sub>1</sub>R, although their efficacies varied. We found that the differences in agonist effects continuously increased over time; for example, for β-arrestin2 recruitment, the fold difference between AngII and (Sar<sup>1</sup>, Ile<sup>4</sup>, Ile<sup>8</sup>)-AngII (SII-AngII) was 1.6-fold at 2 min, which increased to 3.2-fold at 20 min after stimulation (Fig. 1A). G protein activation was monitored by measuring the disassembly of tagged G protein subunits (28-30). For this purpose, we used the TRUPATH BRET biosensor set (31). In contrast with the β-arrestin recruitment assay, the ligands could be divided into two groups on the basis of their ability to activate the G<sub>q</sub> protein (Fig. 1B). These groups are referred to as G<sub>q</sub>-activating and non-G<sub>0</sub>-activating ligands. Members of the latter group are also frequently referred to as β-arrestin-biased agonists. In addition, the G<sub>q</sub>-activating ligands effectively activated other G protein TRUPATH sensors as well (including  $G_{11}$ ,  $G_{i1}$ ,  $G_{i2}$ ,  $G_{i3}$ ,  $G_{oA}$ ,  $G_{oB}$ ,  $G_{12}$ , and  $G_{13}$ ), and some G proteins were also partially activated by the  $\beta$ -arrestin– biased ligands (fig. S3). The activation kinetics of the distinct G protein sensors greatly differed; however, in contrast with the divergent ligand-dependent kinetics of β-arrestin binding, the relative differences between ligand effects for G protein activation were stable over time (Fig. 1, B and C). These data are consistent with previous observations that AT<sub>1</sub>R can be stabilized in multiple active conformations, which may selectively couple to distinct transducers. In addition, our results demonstrate the existence of marked temporal differences, which influence signaling efficacy in a ligand- and

transducer-specific manner and thus shape the extent of the apparent functional selectivity.

Because a substantial pool of receptors is expected to be internalized during the investigated time frame, we assessed how their spatial distribution influenced the temporal aspects of transducer activity. First, we focused on the β-arrestin pathway, where the most prominent temporal differences were observed. To study this question, we overexpressed a dominant-negative form of dynamin2A (Dyn-K44A) to inhibit receptor endocytosis (32). We observed that the agonist-specific β-arrestin2 binding curves converged over time (Fig. 1D), in contrast with the divergent behavior under normal conditions. Furthermore, the ligand-dependent differences in AT<sub>1</sub> R-β-arrestin2 binding were almost completely lost in Dyn-K44Aexpressing cells at later times (Fig. 1D versus Fig. 1A). For example, the prototypical β-arrestin-biased agonist SII-AngII switched from being a weak partial agonist to being a near-full agonist. Concentration-response analysis performed with the values from the area under the curve (AUC) of  $AT_1R-\beta$ -arrestin2 interaction revealed a strong relationship between the efficacy and potency values of the distinct agonists under normal conditions. However, when endocytosis was inhibited, we found almost equal ligand efficacies for β-arrestin2 recruitment (Fig. 1, E and F, and figs. S4 and S5), whereas the potency values of the distinct ligands were not significantly different (fig. S5J).

Next, we verified the effects of receptor endocytosis by applying two additional methodologies to inhibit internalization. First, we used a rapamycin-inducible phosphatidylinositol 4,5-bisphosphate [PtdIns(4,5)P<sub>2</sub>] depletion system (fig. S6), because acute degradation of plasma membrane PtdIns(4,5)P<sub>2</sub> prevents GPCR internalization (25, 33). We found that PtdIns(4,5)P2 depletion did not alter the AngII-stimulated AT<sub>1</sub>R-β-arrestin2 interaction but markedly enhanced the effects of the less efficacious agonists, in a manner similar to that of Dyn-K44A coexpression (Fig. 1, G and H, and fig. S6). We also used a hypertonic sucrose solution, which inhibits clathrin-mediated endocytosis (25, 32, 34). Upon pretreatment of cells with hypertonic sucrose, highly similar effects to those caused by PtdIns(4,5) $P_2$  were observed on  $\beta$ -arrestin2 recruitment (Fig. 1I and fig. S7A). During these experiments, we found that the hypertonic sucrose solution decreased the detected luminescence intensities probably by affecting luciferase activity (fig. S7B). Nevertheless, the administration of hypertonic sucrose had the advantage that no additional construct had to be expressed, making it easy to use in different assays of transducer activation. The inhibition of receptor endocytosis with hypertonic sucrose resulted in similar changes in β-arrestin1 recruitment as those that occurred with  $\beta$ -arrestin2 (Fig. 1J and fig. S7C). In contrast, the activation kinetics of Gq, Gi3, and G12, which are representative members of G protein subfamilies, were only slightly or moderately affected, and the overall differences between ligands in their ability to activate G proteins were not altered significantly (Fig. 1J and fig. S7, D to F). Similarly to hypertonic sucrose, Dyn-K44A coexpression had no substantial effect on Gq sensor activation, and neither the efficacy nor the potency of G<sub>q</sub>-activating ligands was significantly altered (fig. S8). When we calculated the bias factors for G<sub>q</sub>-activating ligands using the operational model (35, 36), AngIV appeared to be a G<sub>q</sub>-biased agonist over time (Fig. 1K). Dyn-K44A overexpression, however, reduced the biased property of AngIV, consistent with the selective effect of Dyn-K44A on the receptor- $\beta$ -arrestin interaction.

Fig. 1. Ligand-specific temporal differences in AT<sub>1</sub>Rβ-arrestin binding are lost upon inhibition of receptor internalization, (A) Real-time measurement of AT<sub>1</sub>R-β-arrestin2 (βarr2) binding upon stimulation with the indicated agonists. (B) Real-time measurement of G<sub>a</sub> protein activation after AT<sub>1</sub>R stimulation with the indicated agonists. (C) Comparative analysis of the temporal variability in ligand effects. The variance in ligand-specific BRET responses was calculated as the squared SD of the responses of all agonists. To highlight the temporal change in the distribution of ligand-specific signals, each variance value was divided by the variance of the initial measurement point (~2 min after stimulus). The corresponding kinetic curves are shown in (A) and (B) and figs. S2A and fig. S3 (A to H). (D) Real-time measurement of  $AT_1R-\beta$ -arrestin2 binding in Dyn-K44A-overexpressing cells. ( $\mathbf{E}$ ) Concentration-response curves of AT<sub>1</sub>R-β-arrestin2 binding with or without Dyn-K44A coexpression, showing AUC values. The corresponding kinetic curves are shown in figs. S4 and S5, and the fitted half-maximal effective concentration (EC<sub>50</sub>) values are shown in fig. S5J. (F) Relationship between the potency and efficacy values of different agonists with and without receptor internalization. Data display the linear correlation under both conditions (Mock,  $r^2 = 0.6624$ ; Dyn-K44A,  $r^2 = 0.5685$ ), but the



slopes of the linear regression curves were significantly different ( $-17.45 \pm 4.708$  versus  $-4.745 \pm 1.506$ , P = 0.0233). The 95% confidence intervals are marked by dotted lines. (G to I) Ligand-dependent extent of β-arrestin2 binding at later times (~20 min). Inhibition of endocytosis was achieved by three independent experimental methods: overexpression of Dyn-K44A (G), \*\*P = 0.0044; Ptdlns(4,5)P<sub>2</sub> depletion with rapamycin (Rapa) (H), \*\*P = 0.0068; and hypertonic sucrose treatment (I), \*P = 0.0179. Levene's tests were performed to evaluate the statistical significance of variances in each distribution, which were conducted on data scaled to their respective averages. Box and whiskers plots, complemented by aligned dot plots, show the distribution of the mean response magnitudes of agonists. Veh, vehicle. (J) Assessment of the extent of β-arrestin1 and G protein recruitment by different ligands with or without receptor endocytosis. Data were processed and displayed as for (G) to (I). \*\*P = 0.0087 for  $\beta$ -arrestin1 ( $\beta$ arr1); P = 0.1 for  $G_q$ ; P = 0.4888 for  $G_{13}$ ; P = 0.9733 for  $G_{12}$ . The corresponding kinetic curves are shown in (A) and (D) (for G); fig. S6B [for (H)]; (A) and fig. S7A [for (I)]; and figs. S2A and S7C, (B) and fig. S7D, figs. S3D and S7D, and figs. S3G and S7F [for (J)]. Except for the concentration-response curves, the ligands were applied at 10 μM. Data in (A) to (F) are means ± SEM of three to 19 experiments. Data are expressed as a percentage of the peak AnglI-induced effect (at 100 nM or 10 μM) of the kinetic curves in the same expression condition, either with or without Dyn-K44A coexpression. Because sucrose altered the luminescence intensities, the changes in the BRET ratio of sucrose-pretreated cells were expressed as a percentage of the AnglI-induced effect after sucrose pretreatment. n.s., not significant. (K) Bias factors  $[\Delta \Delta \log(\tau/K_A)]$  or LogBias] were calculated for the  $G_0$ -activating ligands in the absence (left) or presence (right) of Dyn-K44A by fitting the operational model to the averaged responses observed in each indicated time frame, comparing the  $AT_1R$ - $\beta$ -arrestin2 interaction versus TRUPATH  $G_q$  sensor activation. A negative value indicates a bias toward G protein activation, with AnglI selected as the reference ligand. In the absence of Dyn-K44A, there was a significant negative association between the LogBias factor of AngIV and time [ligand:time interaction P value from (bias factor ~ ligand \* time) linear model: P = 0.000039 after Holm-Šidák correction] but not for other ligands (P values are 0.71 and 0.29 for TRV055 and TRV056, respectively). In the presence of Dyn-K44A, the LogBias factor of the ligands showed no significant time-dependent change (P values are 0.95, 0.094, and 0.094 for AnglV, TRV055, and TRV056, respectively).

We further tested the effect of internalization inhibition at the second messenger level. PtdIns(4,5)P<sub>2</sub> cleavage, a hallmark of the  $G\alpha_{q/11}$ -dependent activation of phospholipase C $\beta$  (PLC $\beta$ ), was monitored upon AT<sub>1</sub>R stimulation with or without Dyn-K44A overexpression using a plasma membrane PtdIns(4,5)P<sub>2</sub> BRET sensor (37). Consistent with the lack of change in G<sub>q</sub> biosensor activation upon hypertonic sucrose treatment, Dyn-K44A overexpression did not alter the relative effects of ligands on PtdIns(4,5)P<sub>2</sub> abundance (fig. S9). We concluded that receptor endocytosis generates the ligand-dependent differences in  $\beta$ -arrestin binding, but it does not alter the inherent ability of the active receptor to induce G protein activity. Thus, non–G<sub>q</sub>-activating ligands retained their bias toward  $\beta$ -arrestin when receptor endocytosis was inhibited; however, their partial agonism in  $\beta$ -arrestin binding developed into full or near-full agonism.

## Differences in ligand-dependent $AT_1R-\beta$ -arrestin2 interactions are primarily caused by the diverse abilities of ligands to stabilize endosomal $AT_1R-\beta$ -arrestin2 complexes

Next, we investigated how receptor endocytosis caused liganddependent differences in  $\beta$ -arrestin binding. We hypothesized that the variability of agonist efficacies in  $\beta$ -arrestin recruitment was the consequence of differences in the amounts of agonist–receptor–βarrestin complexes at endosomes. Thus, we generated cell compartmenttargeted biosensors and monitored  $\beta$ -arrestin recruitment in different compartments, similarly to previous designs (38, 39). We fused the BRET donor enzyme NanoLuc either to a myristoylationpalmitoylation sequence or to Rab5 to target it to the plasma membrane or to early endosomes (PM-NanoLuc and EE-NanoLuc, respectively) and applied these biosensors together with Venustagged β-arrestin2 in bystander BRET measurements (Fig. 2A). After AngII treatment, the BRET signal between PM-NanoLuc and β-arrestin2-Venus first increased and then slightly decreased (fig. S10A), which reflects the plasma membrane translocation and the concomitant trafficking of  $\beta$ -arrestin2–Venus. Accordingly, we measured a slightly delayed increase in the BRET signal between EE-NanoLuc and  $\beta$ -arrestin2–Venus, representing the enrichment of β-arrestin2-Venus at endosomes (fig. S10B). Consistent with these findings, when receptor translocation to endosomes was inhibited by Dyn-K44A (fig. S10, C and D), both the declining phase of the plasmalemmal β-arrestin2 translocation and the endosomal β-arrestin2 translocation were prevented (fig. S10, A and B). Similarly to AngII, all of the other AT<sub>1</sub>R ligands also stimulated plasmalemmal and endosomal β-arrestin2 translocations (Fig. 2, B and C). However, the ligand-dependent differences in plasmalemmal βarrestin2 translocation were significantly smaller compared with the differences in endosomal β-arrestin2 recruitment, and the latter was mainly responsible for the overall variance of the total AT<sub>1</sub>R- $\beta$ arrestin2 interaction (Fig. 2, D and E).

Agonist-dependent endosomal  $\beta$ -arrestin2 recruitment was also visualized by confocal microscopy. First, the formation of intracellular  $\beta$ -arrestin2–Venus–enriched vesicles was assessed in live cells after stimulation with AngII, ST-AngII, or SII-AngII, which have markedly different efficacies in  $\beta$ -arrestin recruitment (Fig. 2F). For the unbiased and high-throughput detection of intracellular fluorescent puncta, a machine learning–based algorithm was applied (fig. S11). Significant differences were observed in the abilities of these ligands to form  $\beta$ -arrestin2–Venus–enriched vesicles (Fig. 2G). AngII stimulated the formation of a greater number of

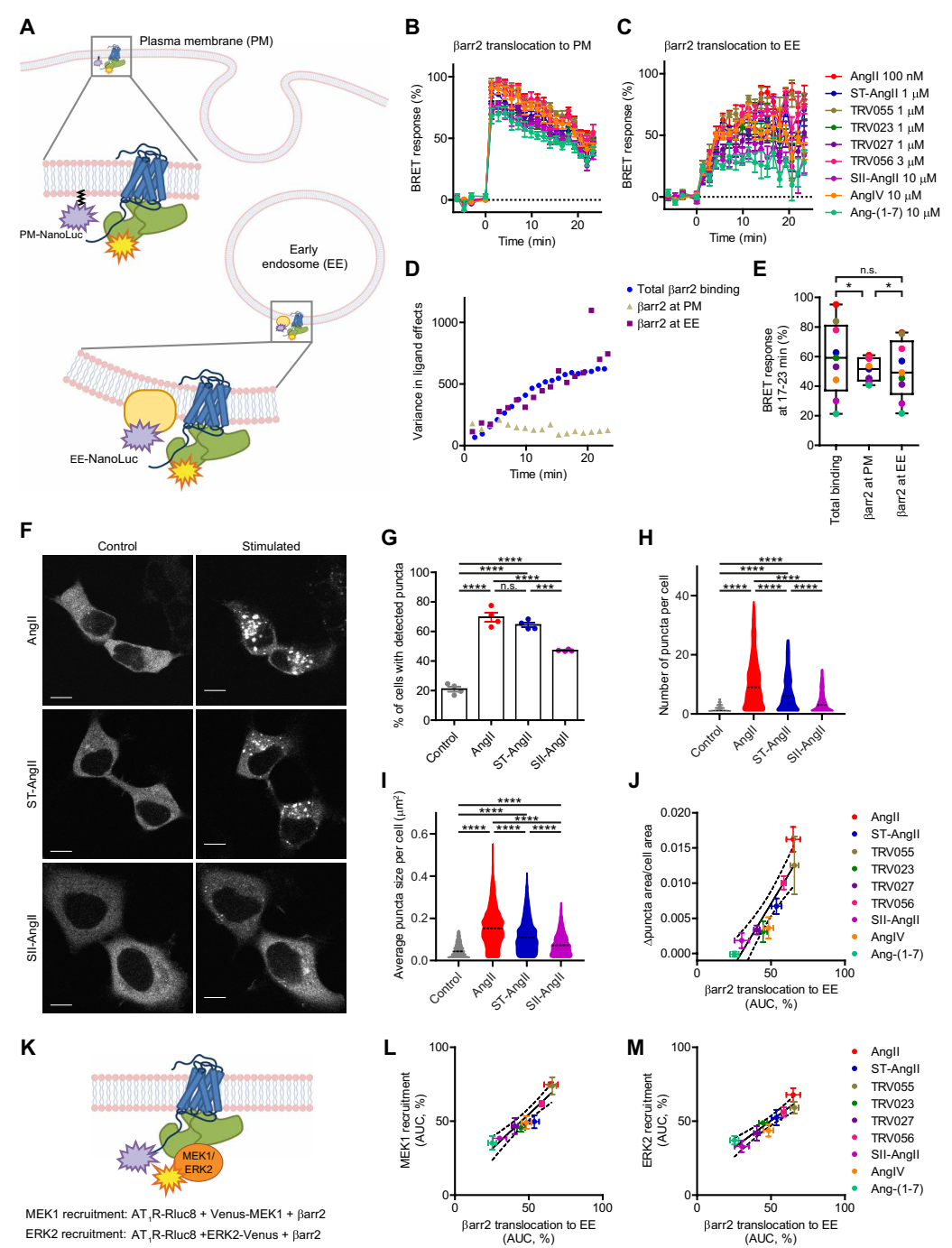
β-arrestin2–Venus–enriched puncta than did ST-AngII or SII-AngII; moreover, the average size of the AngII-stimulated puncta was also significantly greater (Fig. 2, H and I). In addition to live-cell imaging, we performed quantitative analysis on fixed cells with an increased sample size for the full set of agonists. Note that cell fixation caused the formation of artificial intracellular aggregates of β-arrestin2–Venus even in unstimulated cells; however, ligand-specific effects were still detectable. Confocal microscopy revealed a rank order of the agonists highly similar to that revealed by the bystander BRET assay (Fig. 2J). These results verified that the observed temporal bias in β-arrestin recruitment is associated with a spatial bias, because the ligand-dependent differences were characteristic for the endosomal compartment.

Endosomal β-arrestin translocation plays an important role in the β-arrestin-dependent regulation of the mitogen-activated protein kinase (MAPK) signaling cascade (40). Therefore, we also investigated whether the extent of endosomal β-arrestin translocation correlated with the amount of complex formation between AT<sub>1</sub>R, β-arrestin2, and members of the MAPK pathway using previously described BRET assays (Fig. 2K) (41). There was a high degree of correlation between the extent of endosomal β-arrestin translocation and the amount of complex formed with MAPK kinase 1 (MEK1) or extracellular signal-regulated kinase 2 (ERK2), indicating the downstream consequence of the magnitude and location of β-arrestin binding (Fig. 2, L and M, and fig. S12, A to D). The AngIIstimulated signal was significantly decreased upon Dyn-K44A coexpression (fig. S12, E to G), but the phosphorylation of ERK1/2 was not affected (fig. S12, H and I), suggesting that the primary role of endocytosis in the regulation of MAPK signaling by AT<sub>1</sub>R is the dynamic subcellular localization of activated kinases, consistent with earlier studies (42).

## Ligand dissociation rate governs the lifetime of AT<sub>1</sub>R-β-arrestin2 complexes primarily in endosomes

All of the AT<sub>1</sub>R agonists tested stimulated β-arrestin2 recruitment with various kinetics and efficacies; moreover, their signals were differently affected by the inhibition of endocytosis. Our next goal was to explore the intrinsic characteristics of the ligands underlying these differences. To quantify the effects of internalization upon β-arrestin2 recruitment stimulated by the different agonists, we investigated the difference between their maximum effect ( $E_{max}$ ) values with or without Dyn-K44A. We found that the β-arrestin2 signal of the more efficacious ligands was systematically less sensitive to internalization (Fig. 3A). One possible explanation is that they maintain a stable receptor–β-arrestin complex even after receptor trafficking to intracellular compartments. To directly investigate the stability of the  $AT_1R-\beta$ -arrestin2 interaction, we characterized the disassembly of the  $AT_1R-\beta$ -arrestin2 complex. We followed the dissociation of β-arrestin2-Venus from AT<sub>1</sub>R-RLuc after the termination of agonist binding, which was achieved by ligand displacement with the high-affinity, membrane-permeable AT<sub>1</sub>R antagonist candesartan (fig. S13A) (43). The rate of receptor–β-arrestin disassembly ( $k_{dis}$ ) was assessed by using the exponential decay equation. Similar to "internalization sensitivity," the rate of β-arrestin2 detachment from AT<sub>1</sub>R greatly varied between different agonists and displayed a strong inverse correlation with their efficacy values (Fig. 3B). When  $k_{\rm dis}$  values were determined in Dyn-K44A–expressing cells, the values displayed a significant correlation with the corresponding values of the control condition, suggesting that the major

Fig. 2. AT<sub>1</sub>R agonists substantially differ in their ability to induce β-arrestin2 recruitment to endosomes. (A) Schematic illustration of the BRET setups for the compartment-specific monitoring of βarrestin2 translocation. (B and C) Real-time monitoring of  $\beta$ -arrestin2 translocation to the plasma membrane (PM) and to early endosomes (EEs). The indicated saturating ligand concentrations were applied. Data are means ± SEM of four independent experiments. (D and E) Comparison of AT<sub>1</sub>R-β-arrestin2 binding at the indicated compartments. Total β-arrestin2 binding represents the BRET signal between AT<sub>1</sub>R-RLuc and  $\beta$ -arrestin2–Venus (Fig. 1A). (D) Distribution of ligand effects over time, represented by the variance (squared SD) of BRET responses to all agonists. (E) Agonistinduced β-arrestin2 responses at later times (average of BRET responses measured 17 to 23 min after stimulation) are shown. Levene's tests were performed on datasets scaled to their average to compare the variances: (βarr2 at PM versus βarr2 at EE: \*P = 0.0246; total binding versus  $\beta$ arr2 at PM: \*P = 0.0306; total binding versus  $\beta$ arr2 at EE: P = 0.8382). (F to J) Endosomal β-arrestin2 translocation was analyzed by confocal fluorescence microscopy. (F) Representative images of live HEK 293A cells expressing β-arrestin2-Venus before and after stimulation with 10 µM Angll, ST-Angll, or SII-AnglI for 20 to 30 min. Scale bars, 10  $\mu$ m. (G) Quantitative analysis of the formation of agonist-induced,  $\beta$ -arrestin2-enriched vesicles in live cells. Intracellular β-arrestin2-Venus puncta were identified by a machine learning-based algorithm; details are discussed in Materials and Methods and fig. S11. The percentage of cells that contained fluorescent puncta are plotted. All ligands induced a significant response (versus control, \*\*\*\*P < 0.0001) but with varying efficacies (Angll versus SII-Angll, \*\*\*\*P < 0.0001; ST-Angll versus SII-Angll, \*\*\*P = 0.0002; Angll versus ST-Angll, P =0.5284), as determined by one-way ANOVA with Bonferroni post hoc test. Data are means ± SEM of four independent experiments. (H and I) Violin plots display the distribution of the number (H) and average size (I) of intracellular β-arrestin2-



Venus puncta per cell. Only cells with detected puncta from four independent experiments were included in the analysis; 1508, 1584, 1268, and 1040 cells for the control, Angll, ST-Angll, and SII-Angll conditions, respectively, were analyzed. Outliers were identified and removed by the ROUT method (Q = 1%). The amount (H) and the size (I) of the β-arrestin2–Venus–positive puncta were both significantly different between the treatments (\*\*\*\*P < 0.0001), as determined by one-way ANOVA with Bonferroni post hoc test. (J) Correlation between the ligand-specific extent of endosomal β-arrestin2 recruitment as measured by BRET (C) or by confocal microscopic experiments. Image acquisition was performed on paraformaldehyde-fixed cells, which had been stimulated with the same ligand concentrations as those used for the experiments shown in (C). Data are means  $\pm$  SEM of four independent experiments. The ratio of the agonist-induced intracellular puncta area and the whole-cell area was assessed for all AT<sub>1</sub>R agonists and normalized to the ratio of unstimulated cells. These values are plotted against the AUC values from the kinetic curves in (C). Linear regression,  $r^2 = 0.8492$ , \*\*\*P = 0.0004; dotted lines indicate 95% confidence intervals. (**K**) Schematic representation of the BRET assay used to monitor AT<sub>1</sub>R-β-arrestin2–MEK/ERK2 complex formation. (**L** and **M**) Correlation between the extent of endosomal P = 0.0004; are means P = 0.0004; dotted lines indicate same as those used for the experiments in (C). Data are means P = 0.0004; dotted lines are applied were the same as those used for the experiments in (C). Data are means P = 0.0004; for (M): linear regression, P = 0.0

ligand-specific differences were preserved during the process of endocytosis (fig. S13, B and C). Because the observed  $k_{\rm dis}$  values incorporate the dissociation rates of complex reaction steps among agonists, receptors, and β-arrestin molecules, we tested whether the marked differences between ligands were driven by their kinetic binding parameters. We performed competitive ligand-binding measurements to assess the association and dissociation rates of the ligand-receptor interactions ( $k_{\rm on\_LR}$  and  $k_{\rm off\_LR}$  values, respectively), using our previously described *Gaussia* luciferase (GLuc)-based BRET platform (fig. S14 and Table 1) (44). Whereas no significant correlation was found between  $k_{\rm on\_LR}$  and the extent of AT<sub>1</sub>R-β-arrestin2 binding,  $k_{\rm off\_LR}$  showed a similar significant inverse correlation as that of  $k_{\rm dis}$  with the efficacy of the AT<sub>1</sub>R-β-arrestin2 interaction (Fig. 3, C and D). Moreover, the  $k_{\rm off\_LR}$  values, obtained from the direct GLuc-based ligand-binding assay, highly correlated

with the  $k_{\rm dis}$  values of the  $\beta$ -arrestin2 dissociation assay (fig. S13D). These data indicate that the dissociation rate of ligands is a major contributor to the agonist-dependent differences and that only ligands with low  $k_{\rm off\_LR}$  values maintain receptor– $\beta$ -arrestin complexes after their translocation to endosomes.

However, we also observed that  $G_q$ -activating ligands generally displayed greater efficacy than that of biased agonists, regardless of their  $k_{dis}$  values (Fig. 3E). This suggests that G protein–dependent factors influence the quantity of receptor– $\beta$ -arrestin complexes without regulating their disassembly, but they potentially affect their assembly. In this case, balanced agonists should already promote increased  $\beta$ -arrestin binding at the initial phase of signaling. Accordingly,  $G_q$ -activating agonists induced significantly greater responses at 2 min after stimulation than did  $\beta$ -arrestin–biased agonists (Fig. 3F). This early difference in response was not sensitive to Dyn-K44A

Fig. 3. Ligand dissociation rate inversely correlates with the efficacy of the AT<sub>1</sub>R-β-arrestin2 interaction. (A) Correlation between the liganddependent efficacy and internalization sensitivity of AT<sub>1</sub>R-β-arrestin2 binding. The efficacy and degree of internalization sensitivity of each ligand were evaluated from the concentration-response curves shown in Fig. 1E. Internalization sensitivity was quantified by calculating the difference between the  $E_{\text{max}}$  values in the presence or absence of Dyn-K44A. Linear regression,  $r^2 = 0.9643$ , \*\*\*\*P < 0.0001; dotted lines represent 95% confidence intervals. (B) Correlation between the dissociation rate of  $\beta$ -arrestin2-Venus from AT<sub>1</sub>R-RLuc ( $k_{dis}$ ) and the efficacy of AT<sub>1</sub>R- $\beta$ -arrestin2 binding ( $r^2 = 0.5476$ ; \*P = 0.0226). Kinetic curves are shown in fig. S13A. (**C** and **D**) Correlation between the  $E_{\text{max}}$  of AT<sub>1</sub>R- $\beta$ -arrestin2 binding and  $k_{on LR}$  (C) or  $k_{off LR}$  (D).  $k_{\rm off\ LR}$  showed a significant inverse correlation  $(r^2 = 0.4794; *P = 0.0387)$ , whereas  $k_{on LR}$  did not correlate with the extent of β-arrestin2 binding  $(r^2 = 0.3637, P = 0.0982)$ . (**E**) Comparison between the  $\beta$ -arrestin2 binding efficacy of  $G_q$ -activating and non-G<sub>a</sub>-activating ligands. Deviation from the fitted line in (B) was plotted for each G<sub>q</sub>-activating and non- $G_q$ -activating ligand. \*\*\*P = 0.0003 by unpaired two-tailed t test. (F) Comparison of the effects of  $G_q$ -activating and non- $G_q$ -activating ligands on  $AT_1R-\beta$ -arrestin2 binding at early (2 min) and late (20 min) times.  $E_{\text{max}}$  values were fitted on the basis of data depicted in figs. S4 and S5. Data were analyzed by two-way ANOVA with Bonferroni post hoc test. Mock at 2 min: \*\*\*P = 0.0008; Dyn-K44A at 2 min: \*\*\*\*P < 0.0001; Mock at 20 min: \*P = 0.018; Dyn-K44A at 20 min: n.s.). Data are means  $\pm$  SEM.

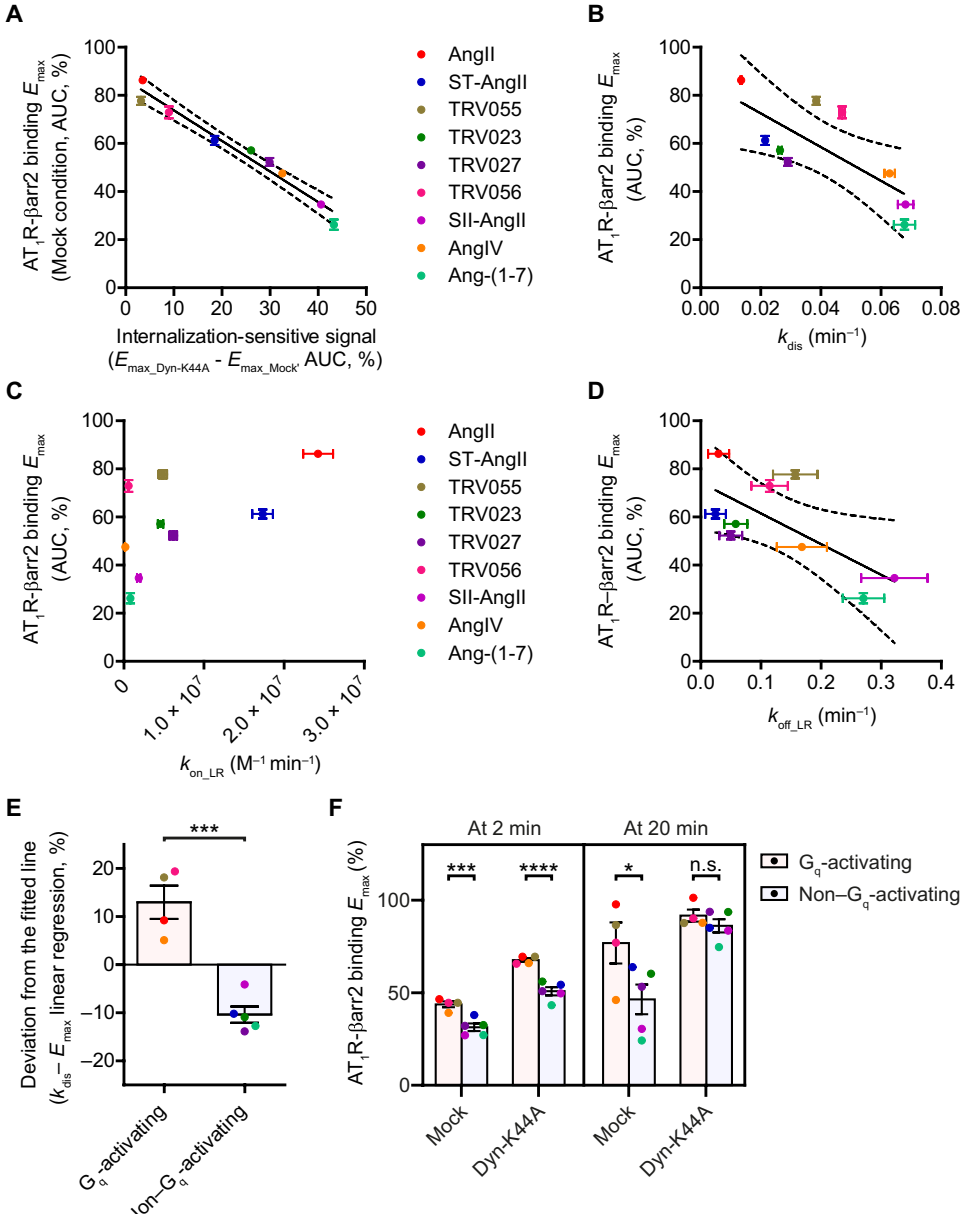


Table 1. Ligand association and dissociation rates determined by the GLuc-based competitive ligand binding assay. The  $k_{\text{on}\_LR}$  and  $k_{\text{off}\_LR}$  values of ligand-AT<sub>1</sub>R interactions are means  $\pm$  SEM of three to five experiments. The corresponding kinetic curves are shown in fig. S14.

	$k_{\text{on\_LR}} (M^{-1} \text{ min}^{-1})$		$k_{ m off\_LR}({ m min}^{-1})$	
	Means	SEM	Means	SEM
Angll	$2.42 \times 10^{7}$	$1.86 \times 10^{6}$	$2.96 \times 10^{-2}$	$1.74 \times 10^{-2}$
ST-Angll	1.73 × 10 <sup>7</sup>	1.28 × 10 <sup>6</sup>	2.46 × 10 <sup>-2</sup>	1.72 × 10 <sup>-2</sup>
TRV055	4.86 × 10 <sup>6</sup>	5.41 × 10 <sup>5</sup>	1.57 × 10 <sup>-1</sup>	3.70 × 10 <sup>-2</sup>
TRV023	$4.57 \times 10^6$	3.44 × 10 <sup>5</sup>	5.83 × 10 <sup>-2</sup>	1.91 × 10 <sup>-2</sup>
TRV027	6.15 × 10 <sup>6</sup>	4.80 × 10 <sup>5</sup>	4.99 × 10 <sup>-2</sup>	1.89 × 10 <sup>-2</sup>
TRV056	5.75 × 10 <sup>5</sup>	5.87 × 10 <sup>4</sup>	1.15 × 10 <sup>-1</sup>	$3.04 \times 10^{-2}$
SII-AnglI	1.85 × 10 <sup>6</sup>	2.14 × 10 <sup>5</sup>	3.22 × 10 <sup>-1</sup>	5.51 × 10 <sup>-2</sup>
AnglV	1.77 × 10 <sup>5</sup>	2.17 × 10 <sup>4</sup>	1.68 × 10 <sup>-1</sup>	4.16 × 10 <sup>-2</sup>
Ang-(1-7)	8.14 × 10 <sup>5</sup>	6.54 × 10 <sup>4</sup>	2.71 × 10 <sup>-1</sup>	3.45 × 10 <sup>-2</sup>

coexpression, consistent with the low proportion of internalized receptors at this time. The extent of  $\beta$ -arrestin recruitment by  $G_q$ -activating agonists was greater even at 20 min after stimulation; however, this difference was diminished by Dyn-K44A coexpression (Fig. 3F). This finding implies that the prolonged effects of G protein activity on  $\beta$ -arrestin recruitment are related to receptor translocation to endosomes.

### G protein activity enhances $\beta\text{-arrestin2}$ recruitment to endosomes

To analyze in greater depth how G protein-dependent regulatory factors govern the spatiotemporal dynamics of  $\beta$ -arrestin binding, we systematically compared the effects of the balanced agonist AngII and the β-arrestin-biased ST-AngII (Fig. 4A), ligands that share almost the same  $k_{\text{off LR}}$  value but have substantially different efficacies for β-arrestin recruitment. To uncover the underlying mechanism, we applied genetic and pharmacological perturbations. We first investigated the effects of a complete blockade of G protein activity in experiments with a G protein knockout CRISPR-Cas9 cell line ( $\Delta$ Gsix:  $\Delta$ G<sub>s/olf</sub>/ $\Delta$ G<sub>q/11</sub>/ $\Delta$ G<sub>12/13</sub>), which express only the G<sub>i/o</sub> subfamily members (45), which were pretreated with the G<sub>i/o</sub> inhibitor pertussis toxin (PTX). In these cells, differences between the effects AngII and ST-AngII were lost, and the extent of βarrestin2 binding to AT<sub>1</sub>R was also markedly reduced (Fig. 4, B and C). We tested whether the G protein-mediated effects were dependent on the spatiotemporal regulation of receptor trafficking. Inhibiting endocytosis by coexpression of Dyn-K44A partially reversed the reduced  $\beta$ -arrestin binding in  $\Delta$ Gsix cells (Fig. 4, B and C), suggesting that G proteins play an important role in modulating the recruitment of  $\beta$ -arrestin2 to endosomes. Consistent with this, bystander BRET measurements confirmed significantly reduced  $\beta$ -arrestin2 recruitment to endosomes in  $\Delta$ Gsix cells in response to either AngII or ST-AngII (Fig. 4D and fig. S15A). Consistent with these findings, quantitative confocal microscopic experiments revealed significantly fewer β-arrestin2-Venusenriched intracellular puncta in AngII-stimulated ΔGsix cells (Fig. 4, E and F).

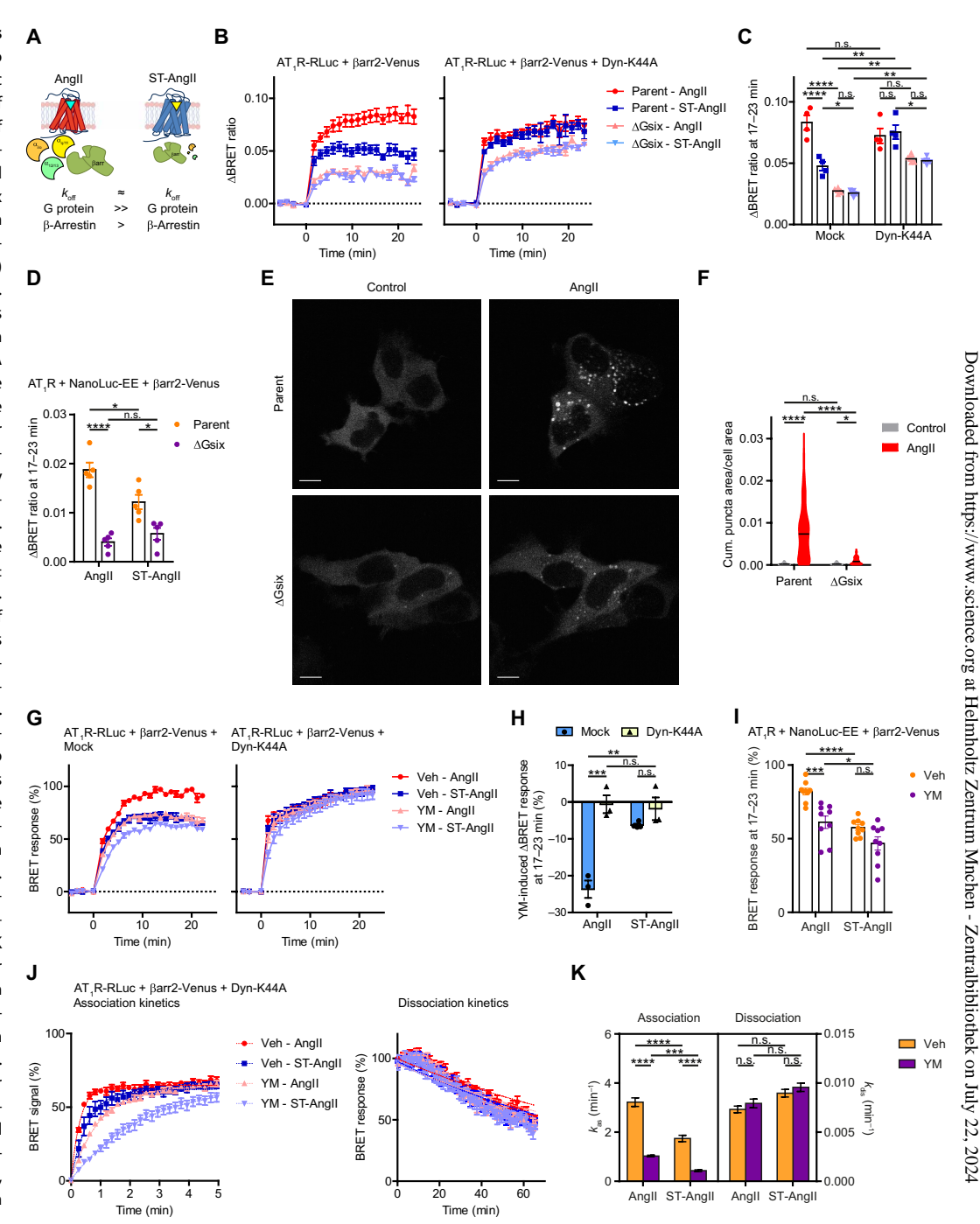
To selectively evaluate the role of  $G_{q/11}$  protein activity, we conducted experiments with a specific  $G_{q/11}$  inhibitor, YM-254890 (YM) (46), after verifying that the drug effectively and selectively

inhibited  $G_{q/11}$  proteins (fig. S15, B to E). In the presence of YM, the AngII-induced response was markedly decreased compared with that in control cells (Fig. 4G). However, this effect was significantly reduced compared with that caused by complete G protein blockade in  $\Delta$ Gsix cells, consistent with a selective effect of YM on  $G_{q/11}$  proteins. Note that YM also exerted a weak but evident effect on the non- $G_{q/11}$ -activating agonist ST-AngII, which may be caused by the inhibitory effect of YM on basal  $G_{q/11}$  activity (fig. S15, B and C). Similarly to what was observed in  $\Delta$ Gsix cells, inhibiting endocytosis reduced the effect of  $G_{q/11}$  inhibition on  $AT_1R-\beta$ -arrestin2 binding (Fig. 4, G and H). Accordingly, pretreatment with YM decreased the AngII-induced recruitment of  $\beta$ -arrestin2 to endosomes in bystander BRET measurements (Fig. 4I), underscoring the importance of the endosomal receptor pool in the lasting effects of G protein activity on  $\beta$ -arrestin recruitment.

Because our earlier findings (Fig. 3F) suggested that  $G_{q/11}$  activity may affect the assembly of the AT<sub>1</sub>R-β-arrestin2 complex, we determined the association kinetics with high temporal resolution in the presence or absence of YM and calculated the observed association rate constant ( $k_{as}$ ). We used Dyn-K44A–coexpressing cells for our measurements to exclude any influence of receptor endocytosis on the maximal signal (considering that a reduced maximal value may cause a falsely high  $k_{as}$  constant upon fitting one-phase association curves). We found that AngII-induced AT<sub>1</sub>R-β-arrestin2 binding resulted in a significantly greater  $k_{as}$  value compared with that induced by ST-AngII and that YM substantially decreased these values. In contrast, the  $k_{dis}$  value was not significantly affected by YM, supporting the conclusion that G protein activity predominantly affects the assembly rather than the disassembly of the receptor-β-arrestin complex.

We further used subcellular compartment–specific inhibitors of  $G\alpha_{q/11}$  signaling (47) to characterize the effects of G protein activity in different compartments (fig. S16). Whereas the plasma membrane–targeted  $G\alpha_{q/11}$ -scavenger protein RGS-CAAX (GRK2-RGS fused to H-Ras–CAAX) inhibited both the early and late phases of the AT<sub>1</sub>R- $\beta$ -arrestin2 interaction, the endosome-localized RGS-FYVE (GRK2-RGS fused to tandem endofin FYVE domains) only decreased the late phase of the AngII-induced signal. These findings are consistent with previous data showing that the plasmalemmal activation of  $G\alpha_{q/11}$  is necessary for its endosomal activity (47) and

Fig. 4. G protein activity promotes the recruitment of  $\beta$ -arrestin2 to AT<sub>1</sub>R at endosomes. (A) Schematic comparison of the characteristics of Angll and ST-Angll. (B) Monitoring of  $\beta$ -arrestin2-Venus binding to AT<sub>1</sub>R-RLuc in parental and PTX-pretreated (PTX of 100 ng/ml for 20 hours)  $\Delta$ Gsix HEK 293A cells after treatment with 10 μM Angll or ST-Angll. Kinetic measurements were performed with Mock (left) and Dyn-K44A-expressing cells (right). (C) Statistical comparison of the changes in BRET ratios at later times (17 to 23 min after stimulation) by three-way ANOVA with Bonferroni post hoc test. Only the biologically meaningful comparisons are shown. Data are means ± SEM of four independent experiments. (D) Monitoring of β-arrestin2 recruitment by bystander BRET measurements in parental and  $\Delta$ Gsix cells at later times. The corresponding kinetic curves are shown in fig. S15A. Data are means  $\pm$ SEM of five independent experiments. (E) Representative live-cell images of parental and PTX-pretreated ΔGsix cells before and after stimulation with Angll. Scale bars, 10 µm. Data are representative of four independent experiments. (F) Quantitative analysis of live-cell images of untreated and stimulated (20 to 30 min) cells; 90, 194, 301, and 396 cells with similar  $\beta$ -arrestin2–Venus abundance were analyzed for each condition. Outliers were identified and excluded from the data with the ROUT method (Q = 1%). Data are from four independent experiments. (G) Kinetics of β-arrestin2-Venus recruitment to AT<sub>1</sub>R-RLuc in HEK 293T cells pretreated with vehicle or 100 nM YM-254890 (YM) for 40 min under mock (left) or Dyn-K44A-expressing (right) conditions. Data are from three or four independent experiments. (H) YM-dependent relative changes at later times. Data are normalized to vehicle pretreatment for each ligand. (I) Endosomal  $\beta$ -arrestin2 recruitment in vehicle- or YMpretreated cells upon AnglI stimulation, as measured by bystander BRET. Data are means  $\pm$  SEM of nine experiments.



(J) Monitoring of the effects of YM on the assembly (left) and disassembly (right) of AT<sub>1</sub>R- $\beta$ -arrestin2 complexes. Left: The association between  $\beta$ arr2-Venus and AT<sub>1</sub>R-RLuc was monitored in Dyn-K44A-coexpressing cells. Temporal resolution was enhanced through the use of injectors to apply stimuli. One-phase association binding curves were fitted to assess the observed association rate constants ( $k_{as}$ ). Right: After 26 min of treatment with 10  $\mu$ M agonist, cells were treated with 30  $\mu$ M candesartan (represented as the zero time point). One-phase dissociation curves were fitted to the data points to assess  $k_{dis}$  values. Data are means  $\pm$  SEM of three or four experiments. (**K**) Statistical comparison of  $k_{as}$  and  $k_{dis}$  values, obtained from the kinetic curves in (J). Data are means  $\pm$  SEM. For all panels, 10  $\mu$ M Angll and ST-Angll were applied. Except for (C), statistical evaluation was performed by two-way ANOVA with Bonferroni post hoc test. \* $P \le 0.05$ , \*\* $P \le 0.01$ , \*\* $P \le 0.001$ , and \*\*\* $P \le 0.001$ ; n.s., P > 0.05.

directly imply a substantial role for G protein activity in the recruitment of  $\beta$ -arrestin2 to endosomes.

 $G\alpha_{q/11}$  activity also leads to PtdIns(4,5)P<sub>2</sub> hydrolysis, which may decrease the extent of receptor internalization (25) and thus may further contribute to enhanced  $\beta$ -arrestin2 recruitment. Note that  $\beta$ -arrestin2 binding measurements require overexpression of  $\beta$ -arrestin2, which may affect the amount of PtdIns(4,5)P<sub>2</sub> at the plasma membrane (48, 49). In the presence of overexpressed  $\beta$ -arrestin2, agonist-stimulated PtdIns(4,5)P<sub>2</sub> depletion was only transient (fig. S17, A and B), and there was no substantial difference in the extent of receptor internalization stimulated by the distinct ligands (fig. S17, C to F). These results also argue against the differences in  $\beta$ -arrestin2 binding being attributed to distinct ligand-dependent internalization properties.

These findings indicate that G protein activity increases the association rate of the  $AT_1R$ – $\beta$ -arrestin2 interaction, whereas it does not significantly affect its dissociation rate, which results in an overall increased interaction. Because the prolonged effects of G protein activity depend on receptor endocytosis, we hypothesize that G proteins might promote the assembly of  $AT_1R$ – $\beta$ -arrestin2 complexes at endosomes through a mechanism that remains to be elucidated.

## Agonist-specific recruitment of $\beta$ -arrestin to GPCRs with class B-type binding is generally dependent on endocytosis

GPCRs are traditionally divided into two classes (A and B) on the basis of the stability of their β-arrestin binding (50). AT<sub>1</sub>R belongs to class B receptors, which form a stable complex with  $\beta$ -arrestin2 at the endosomal compartment, where ligand-dependent differences in  $\beta$ -arrestin2 binding mostly emerged in our earlier experiments. To address the question of whether the observed findings can generally characterize the β-arrestin binding of class B GPCRs, we extended our investigations to another prototypical class B receptor, the V<sub>2</sub>R (50). We characterized the recruitment of β-arrestin2 to V<sub>2</sub>R induced by two endogenous agonists, arginine vasopressin (AVP) and oxytocin (OT) with or without Dyn-K44A coexpression (Fig. 5, A to D, and fig. S18, A and B). We found that these ligands exhibited significant, time-dependent differences in the  $V_2R-\beta$ arrestin2 interaction, which were abolished in the absence of endocytosis. Consistently, compartment-specific measurements revealed that AVP and OT were similarly effective in stimulating the translocation of  $\beta$ -arrestin2 to the plasma membrane but that OT was significantly less efficacious in promoting its endosomal translocation (Fig. 5, E to G).

To further demonstrate the integral role of the endosomal compartment in determining the agonist-specific extent of βarrestin binding, we performed experiments with a prototypical class A GPCR, the  $\beta_2$ AR, which is incapable of endosomal  $\beta$ -arrestin recruitment. We hypothesized that the artificial induction of an endosomal pool of β<sub>2</sub>AR-β-arrestin2 complexes might augment differences between distinct  $\beta_2AR$  agonists in the recruitment of  $\beta$ arrestin2. To test this hypothesis, we used a mutant form of  $\beta_2AR$ that is converted to a class B receptor through the incorporation of C-terminal phosphorylation sites ( $\beta_2$ AR-3S) (Fig. 6A) (51). In the case of wild-type (WT)  $\beta_2$ AR, we found that three tested  $\beta_2$ AR agonists led to similar recruitment of β-arrestin2 (Fig. 6B). However, we found that the extent of the interaction between mutant  $\beta_2AR-3S$ and β-arrestin2 was not only increased in general but that marked differences emerged between the effects of ligands (Fig. 6C). Moreover, if we inhibited receptor internalization with Dyn-K44A, then

these differences were almost completely eliminated (Fig. 6, D and E, and fig. S18, C to F), indicating that the ligand-dependent differences with  $\beta_2AR$ -3S arose from the distinct abilities of the  $\beta_2AR$  agonists to induce endosomal  $\beta$ -arrestin recruitment. These results imply that receptor endocytosis determines the amount of agonist-induced GPCR– $\beta$ -arrestin complexes that form and act as a general orchestrator of the temporal effects of kinetic ligand parameters and spatial factors.

## Quantitative modeling reveals kinetic factors that regulate the endosomal recruitment of $\beta$ -arrestin

Our results suggest that ligand-dependent differences in the binding of  $\beta$ -arrestin to class B GPCRs predominantly manifest in intracellular compartments, as we summarize in our simplified model (Fig. 7). However, precise experimental identification of the underlying internalization-sensitive molecular factors and their selective analyses face technical limitations. To overcome these shortcomings and to investigate our concept with an independent approach, we constructed a kinetic mathematical model of GPCR signaling that enabled individual analysis of the relevant parameters in a compartment-specific manner.

We formulated ordinary differential equations (ODEs) to describe how the G protein activation and  $\beta\text{-}arrestin$  binding of receptors develop over time upon agonist stimulation. We assembled a complete modeling framework (fig. S19), in which receptor internalization is also included. The reaction rate constants and the initial concentrations of molecules were either chosen from previously introduced mathematical models of GPCR signaling and published experimental data or were determined on the basis of rational assumptions (tables S1 and S2) (52–56). Our simulations yielded  $G_q$  activity and  $\beta\text{-}arrestin$  binding concentration-response curves and displayed the time course of downstream signaling events mediated by  $G_q$  proteins (fig. S20).

To investigate our experimental findings, we performed simulations that examined the spatiotemporal aspects of  $\beta$ -arrestin binding and its relationship with the ligand dissociation rate constant ( $k_{\text{off LR}}$ ). A well-known difference between the local regulation of GPCR signaling at endosomes is the relative rates of receptor phosphorylation and dephosphorylation compared with those at the plasma membrane (57-60). To model this, we set the receptor phosphorylation rate at the plasma membrane to be greater than that at endosomes, and we selectively evaluated the number of β-arrestin-bound receptors at the two different compartments. Consistent with our experimental results, a ligand with a greater  $k_{\text{off\_LR}}$  value induced less β-arrestin binding and displayed a different kinetic profile (Fig. 8A). In addition, the  $k_{\text{off LR}}$ -dependent differences were more prominent in the intracellular compartment than at the plasma membrane (Fig. 8, B and C). In agreement with these findings, in silico inhibition of receptor internalization greatly reduced the effects of the dissociation rate constant (Fig. 8, A to D). These simulations reveal that the experimental correlation between  $k_{\text{off LR}}$  and  $E_{\text{max}}$  implies a direct causation and confirm that the effects of  $k_{\text{off\_LR}}$  are endocytosis

β-Arrestin binding is modulated by numerous cellular regulatory mechanisms that affect the phosphorylation state of receptors or, otherwise, change the affinity of the receptor– $\beta$ -arrestin complex. To test whether such systemic factors also influence  $k_{\rm off\_LR}$ -dependent effects, we perturbed the reaction rate constants of the  $\beta$ -arrestin binding pathway. The  $k_{\rm off\_LR}$ -specific differences in  $\beta$ -arrestin

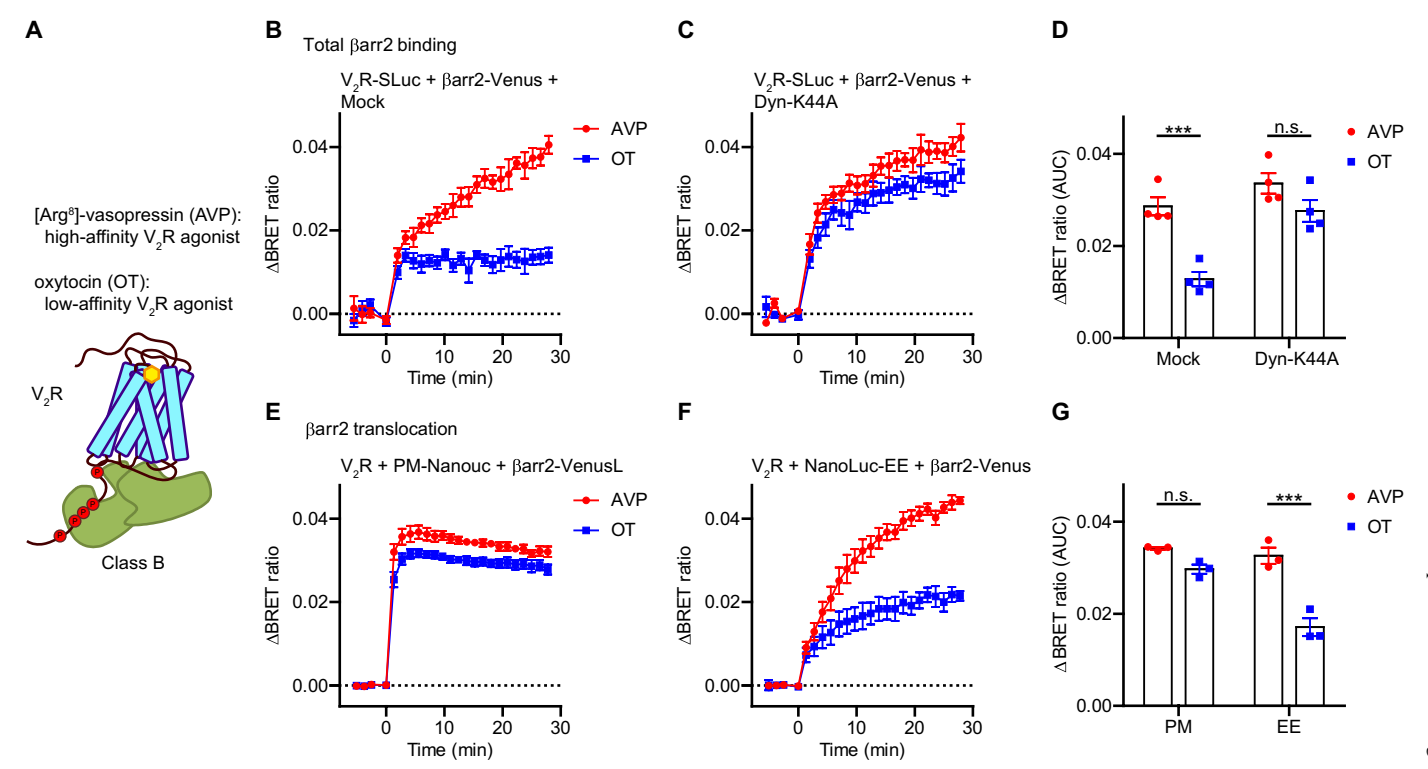


Fig. 5. Oxytocin and vasopressin induce different extents of  $V_2R-\beta$ -arrestin2 binding at endosomes but not at the plasma membrane. (A) Schematic representation of the class B-type  $\beta$ -arrestin binding of  $V_2R$  and descriptions of the two endogenous  $V_2R$  ligands used. (B and C) Kinetic measurements of the binding of  $\beta$ -arrestin2–Venus to  $V_2R$ -SLuc in response to 10 μM AVP and 30 μM OT in the absence (B) and presence (C) of Dyn-K44A. The concentration-response curves for AVP and OT are shown in fig. S18 (A and B). (D) AUC values of the curves shown in (B) and (C) were analyzed to statistically compare the effects of the indicated ligands. \*\*\*P = 0.0003 for Mock and P = 0.1232 for Dyn-K44A—coexpressing cells. (E and F) Real-time monitoring of the translocation of  $\beta$ -arrestin2 to the PM and to EEs by bystander BRET measurements. (G) Statistical comparison of AVP- and OT-induced  $V_2R-\beta$ -arrestin2 binding at the indicated compartments. AUC values from (E) and (F) are shown. Data are means  $\pm$  SEM of three or four independent experiments and were analyzed by two-way ANOVA with Bonferroni post hoc test. \*\*\*P = 0.0001 at EEs and P = 0.1076 at PM.

recruitment were highly sensitive to changes in any of the investigated reaction rates (Fig. 8E and fig. S21). An increased relative proportion of phosphorylation at the endosomes compared with that at the plasma membrane (by decreasing the phosphorylation rate at the plasma membrane, decreasing the dephosphorylation rate at the endosomes, increasing the phosphorylation rate at the endosomes, or increasing the dephosphorylation rate at the plasma membrane) reduced the  $k_{\text{off\_LR}}$ -specific differences. In the case of receptor- $\beta$ -arrestin binding parameters, both an increase and a decrease in the stability of the receptor-β-arrestin complex led to decreased koff LR-specific differences. Moreover, we found that, in the absence of receptor endocytosis, the difference between a ligand with a low  $k_{\text{off LR}}$  value and a ligand with a high  $k_{\text{off LR}}$  value was generally less affected by our perturbations (Fig. 8E, right). These findings suggest that the modulation of the relationship between the  $k_{\text{off LR}}$  value of a ligand and β-arrestin2 efficacy may serve as an important way to fine-tune signaling. On the other hand, changes in the ligand dissociation rate did not affect the maximal extent of G protein activation (Fig. 8F), indicating that kinetic ligand parameters have disparate effects on distinct receptorstimulated pathways. In contrast with  $k_{\text{off LR}}$ , alterations in the  $k_{\text{on LR}}$ of a ligand were not associated with marked changes in the efficacy of the investigated transducers (Fig. 8, F and G).

To systematically analyze the role of  $k_{\rm off\_LR}$  in apparent pathway selectivity, we ran simulations with a set of test agonists with gradually altered  $k_{\rm off\_LR}$  values and calculated a bias factor to quantify

their relative preference toward  $G_q$  activation relative to  $\beta$ -arrestin binding (Fig. 8H). In the presence of receptor trafficking, the  $k_{\rm off\_LR}$  value emerged as a decisive attribute of ligands in their "functional selectivity." However, without internalization, the calculated bias remained almost completely unaltered by  $k_{\rm off\_LR}$ , further highlighting the role of compartmentalization in functionally selective signaling.

#### **DISCUSSION**

Here, we demonstrated that functionally selective signaling of GPCRs is a concerted interplay among the intrinsic characteristics of the agonist-activated receptor structure (ligand bias), kinetic parameters (temporal bias), and spatial factors (location bias) that are strongly connected and strictly coordinated by the phenomenon of receptor endocytosis. We applied a diverse set of experimental and in silico approaches to unveil how receptor trafficking organizes these "types of bias" and displayed our results with AT<sub>1</sub>R, a prototypical GPCR that exhibits biased signaling. We found that inhibiting receptor internalization eliminated the differences between the AT<sub>1</sub>R-β-arrestin binding efficacies of distinct agonists, including those classically considered to be biased and balanced ligands. We provided mechanistic insights into the marked effects of receptor trafficking by showing that ligand-dependent regulatory factors of β-arrestin binding were mainly exerted at the endosomal compartment. We extended our findings to V<sub>2</sub>R, proposing that a common

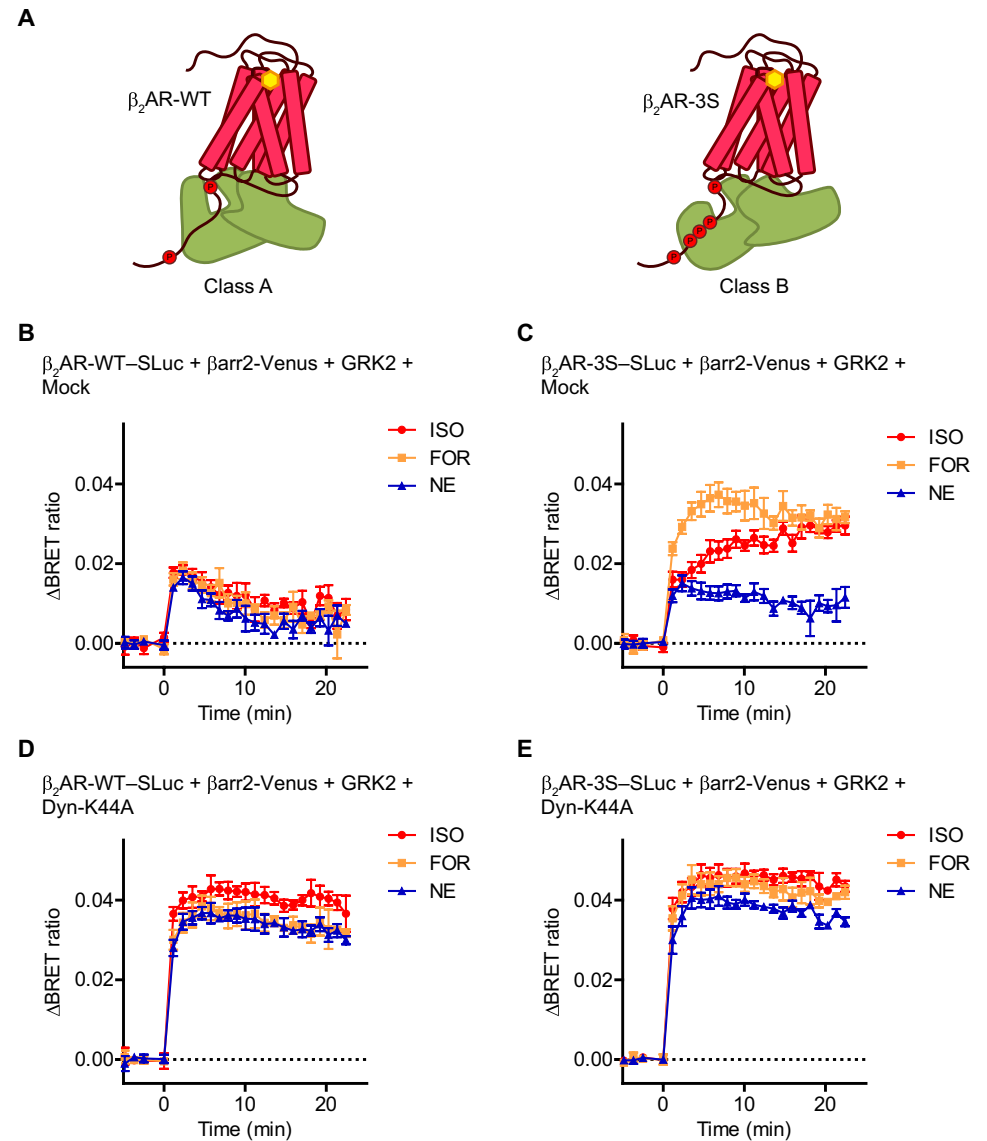
mechanism underlying the differing  $\beta$ -arrestin recruitment efficacies of ligands for GPCRs with class B–type binding lies in their induction of varying degrees of interaction at endosomes but not at the plasma membrane.

Despite great research progress regarding "compartmentalized signaling" and "biased signaling," the molecular links between these two phenomena remain poorly understood. On the other hand, their joint translational potential was highlighted by Eiger *et al.* (23), who demonstrated that endocytosis is necessary for a  $\beta$ -arrestin–biased agonist to exert its anti-inflammatory effects in mice. These results imply the unexploited possibility to rationally design biased drugs with defined spatiotemporal pharmacological profiles. Our experimental work addressed this concept, and we identified the principal characteristics of ligands that determine signaling efficacy and the extent of functional selectivity in a compartment-specific manner.

First, we found that a greater ligand dissociation rate was linked with faster disassembly of the agonist–receptor– $\beta$ -arrestin complexes and thus decreased the total amount of  $\beta$ -arrestin–bound

receptors. Our results regarding the marked influence of ligand dissociation rate constant on the overall β-arrestin binding efficacy are supported by previous observations made with other GPCRs (19, 61, 62). However, a study by Mösslein et al. (63) contradicts this hypothesis, because the authors found no effect of  $k_{\text{off}}$  LR on receptor β-arrestin complex stability during the investigation of β<sub>2</sub>-adrenergic and μ-opioid receptors, which exhibit class A-type β-arrestin binding (cannot recruit  $\beta$ -arrestin at endosomes). Here, we resolved this apparent discrepancy, because we not only verified that  $k_{\text{off LR}}$  regulates the amount of receptor-β-arrestin complexes but also demonstrated that mainly the endosomal pool is affected by this ligand kinetic parameter. Specifically, ligands with large  $k_{\text{off LR}}$  values failed to maintain a stable receptor-β-arrestin interaction after translocation to endosomes. Consistent with the study of Mösslein et al., we found no differences between low- and high-affinity agonists of the WT β<sub>2</sub>AR but did see differences with a phosphorylation site-engineered mutant that has class B-type β-arrestin binding properties.

Fig. 6. Artificial induction of endosomal  $\beta$ arrestin binding of \$\beta\_2\$AR generates ligandspecific differences in  $\beta$ -arrestin2 recruitment. (A) Schematic representation of the  $\beta$ -arrestin binding properties of the WT and the phosphorylation site-engineered mutant (3S) β<sub>2</sub>AR. (**B** and **C**) Kinetics of the interactions between  $\beta$ -arrestin2– Venus and WT β<sub>2</sub>AR-SLuc (B) and β<sub>2</sub>AR-3S-SLuc (C) in response to stimulation with 30 µM formoterol (FOR), 30  $\mu$ M isoproterenol (ISO), and 300  $\mu$ M norepinephrine (NE), concentrations that exert maximal  $\beta$ -arrestin2 binding. (**D** and **E**) Measurement of  $\beta$ -arrestin2 binding to the WT and the 3S-mutant receptors in Dyn-K44A-expressing cells. The corresponding concentration-response curves for the experiments shown in (B) to (E) are shown in fig. S18 (C to F). Data are means  $\pm$  SEM of three or four experiments.



Second, we showed that balanced agonists stimulated receptor- $\beta$ -arrestin interactions to a greater extent than did  $\beta$ -arrestin-biased agonists and that ligand bias per se was not affected by the inhibition of receptor trafficking. However, we found that G protein activity facilitated the AT<sub>1</sub>R- $\beta$ -arrestin interaction but that the effects of G protein activity on  $\beta$ -arrestin recruitment endured only in the context of receptor internalization. In contrast with the ligand dissociation rate constant ( $k_{\rm off\_LR}$ ), which mainly reflects the disassembly of receptor- $\beta$ -arrestin complexes ( $k_{\rm dis}$ ), we found that G protein activity mostly affected their association ( $k_{\rm as}$ ). The underlying molecular mechanism may be that  $G_q$ - versus non- $G_q$ -activating agonists can engage different sets of GRKs (7), and it is tempting to speculate that G proteins may directly activate GRKs at endosomes as well.

To summarize these preceding points, our results indicate that the variance in the amount of receptor– $\beta$ -arrestin complex at endosomes, stimulated by distinct agonists, results from a multifactorial process. Agonists may vary in their ability to sustain receptor– $\beta$ -arrestin complexes after translocation from the plasma membrane and potentially in recruiting  $\beta$ -arrestins to receptors at endosomes. However, the selective experimental investigation of receptor– $\beta$ -arrestin complexes

that are directly formed at endosomes and the role of G proteins in this mechanism now face unresolved technical difficulties.

Which special properties of the endosomal compartment can contribute to the locally different regulation of β-arrestin recruitment, and how do they connect ligand characteristics with location bias? Our modeling approach showed that the relative activity of phosphorylation and dephosphorylation mechanisms is a possible main determinant of the magnitude of β-arrestin binding. Several observations from current and previous studies imply that dephosphorylation mechanisms dominate at endosomes because of the relatively greater extent of phosphatase activity and the reduced extent of GRK activity (58-60) in contrast with those at the plasma membrane, where the relatively increased abundance of different GRK isoforms markedly shifts the regulatory reactions in favor of receptor phosphorylation (64). Furthermore, not only does the quantity of phosphorylated receptors matter, but the sequence of the phosphorylation residues, also known as the phosphorylation barcode, has equally important effects on the extent, kinetics, and conformation of β-arrestin binding. Evidence suggests that distinct ligands have different phosphorylation barcodes, which manifest in

Fig. 7. Model of the role of endocytosis in the diverse effects of agonists on  $\beta$ -arrestin recruitment to GPCRs. A simplified model illustrates the spatiotemporal regulation of agonist efficacy in receptor-β-arrestin interactions. Agonists that elicit similar degrees of β-arrestin translocation to the receptor at the plasma membrane may cause substantially different extents of βarrestin recruitment at endosomes (depicted by wireless symbols). The primary factors responsible for these varying effects at endosomes are the ligand dissociation rate and G protein activity, which influence the disassembly and the assembly of the receptor-β-arrestin complex, respectively. Because differences become apparent at the endosomal level, the efficacy of β-arrestin recruitment by these agonists becomes equalized when endocytosis is inhibited.

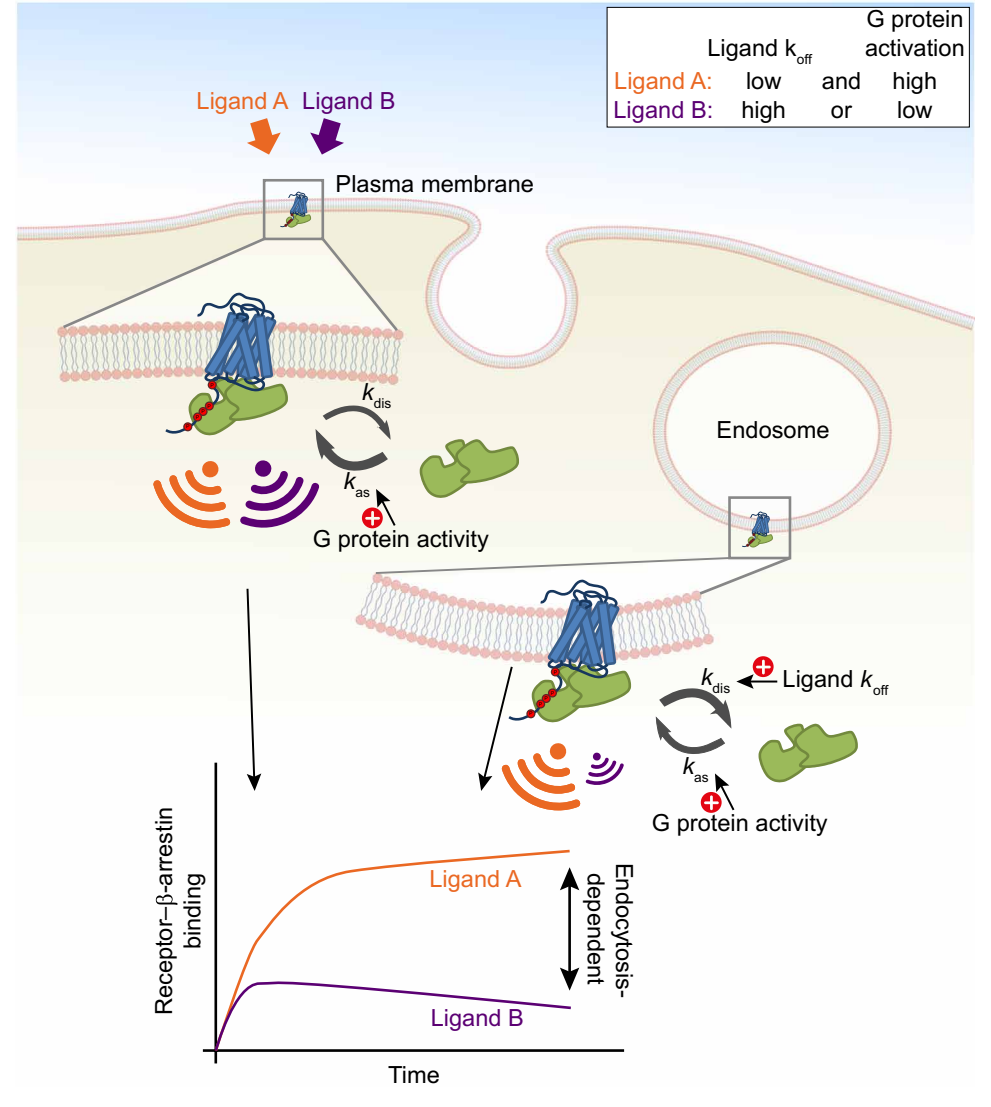
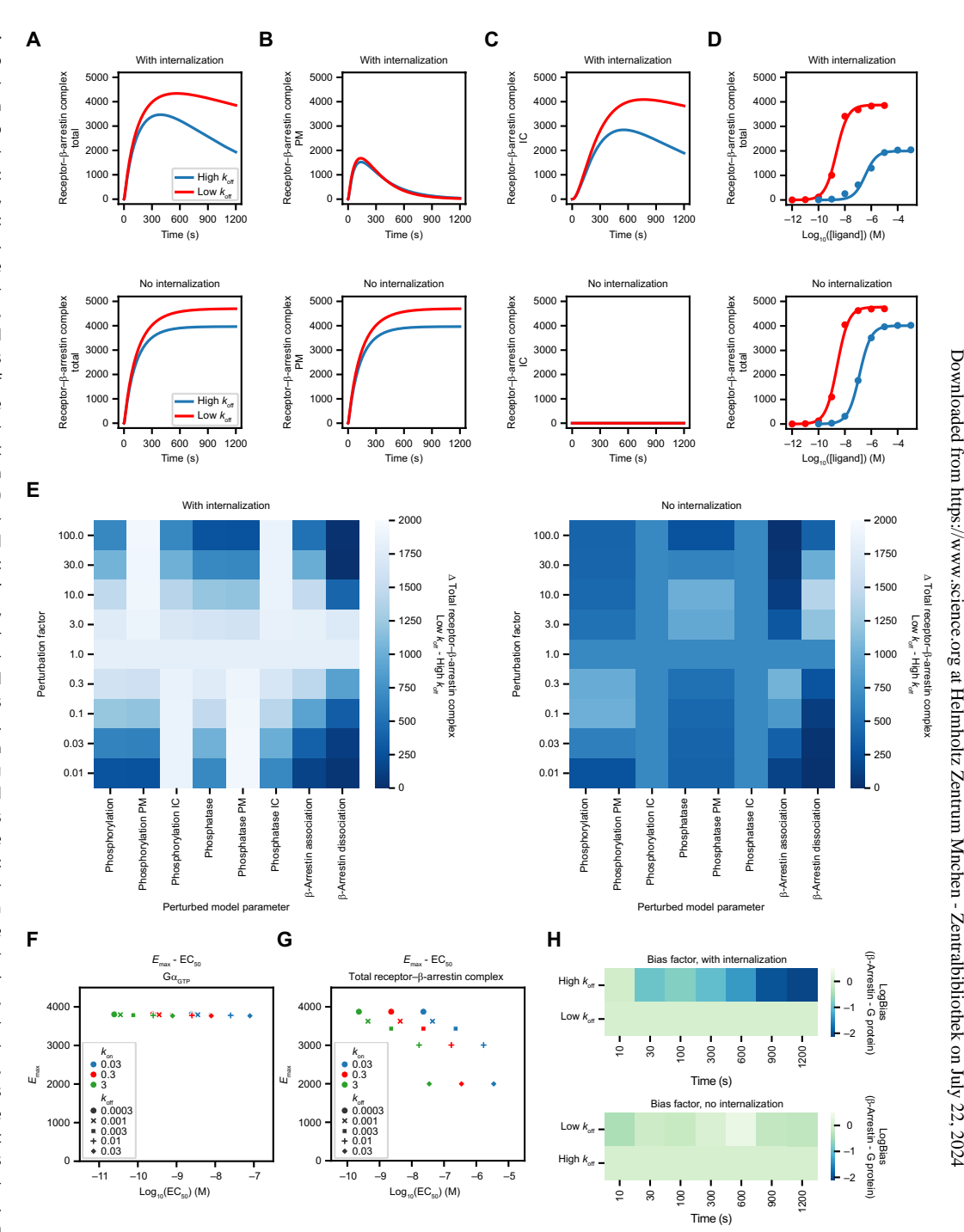


Fig. 8. Quantitative kinetic modeling reveals mechanistic insights into spatiotemporal bias. (A to C) Simulated time-course profiles of  $\beta$ -arrestin binding upon stimulation with two agonists, which only differ in their receptor dissociation rate constants ( $k_{\text{off LR}}$ : reactions 2, 4, 6, 8, 10, 12, 14, 16, 18, 20, 22, 24, 52, 54, 56, and 58; "low k<sub>off</sub>":  $k_{\text{off\_LR}} = 0.0003$ ; "high  $k_{\text{off}}$ ":  $k_{\text{off\_LR}} = 0.03$ ). Top: Simulated curves in the presence of receptor trafficking. Bottom: Receptor internalization rate (reactions 38, 39, and 40) was set to zero. (A) Total amount of β-arrestin-bound receptors in the presence (top) or absence of endocytosis (bottom). (B and C) The number of β-arrestin-bound receptors at the plasma membrane (B) or at the endosomal compartment (C) in the presence (top) or absence (bottom) of endocytosis. Total β-arrestin binding: molecules 10, 11, 12, 13, 14, and 15; plasmalemmal β-arrestin binding: molecules 10, 11, and 12; intracellular B-arrestin binding: molecules 13, 14, and 15. (D) Simulated concentrationresponse curves of the same two agonists shown in (A) to (C). The total number of β-arrestin-bound receptors at 20 min after stimulation is shown. (E) Effect of perturbation of the reaction rate constants of the  $\beta$ -arrestin binding pathway. Simulations were performed by multiplying the initial rate constants of the investigated reactions with the indicated factors (phosphorylation PM: reaction 30; phosphorylation IC (intracellular): reaction 50; phosphorylation IC PM: reactions 30 and 50; phosphatase PM: reactions 25, 27, and 29; phosphatase IC: reactions 47, 48, and 49; phosphatase IC PM: reactions 25, 27, 29, 47, 48, and 49; β-arrestin association: reactions 35, 36, 37, 44, 45, and 46; βarrestin dissociation: reactions 32, 33, 34, 41, 42, and 43). The total numbers of β-arrestin-bound receptors were assessed in systems with or without internalization for the same ligands as those shown in (A) to (D), and the difference of the 20-min values is plotted. The results for each ligand are shown in fig. S21. (F and G) Concentration-



response curves were simulated for the larger set of test ligands with different  $k_{\text{on\_LR}}$  and  $k_{\text{off\_LR}}$  values, which are indicated by the colors or the shape of symbols, respectively ( $k_{\text{on\_LR}}$ : reactions 1, 5, 9, 13, 17, 21, 51, and 55).  $E_{\text{max}}$  and EC<sub>50</sub> values are plotted on the y and x axes, respectively. The number of activated G proteins (molecules 23 and 33) (F) and the total amounts of receptor- $\beta$ -arrestin complexes were assessed (G) and are shown after perturbation of the  $k_{\text{off\_LR}}$  and  $k_{\text{on\_LR}}$  values of the agonists. (H) Heatmaps visualize the time dependence of the degree of G protein bias in the presence (top) or absence (bottom) of receptor trafficking. The extent of bias [ $\Delta\Delta\log(\tau/K_A)$  or LogBias] toward  $\beta$ -arrestin recruitment versus G protein activation was quantified with the operational model, and the agonist with the low  $k_{\text{off}}$  value was set as the reference ligand.

functionally selective signaling outcomes (65–67). Moreover, ligands may be biased regarding their endosomal GRK activation profiles, which further contributes to location bias (68). The distinct lipid composition of intracellular membranes, such as the absence of PtdIns(4,5)P<sub>2</sub>, adds another layer of complexity to the endosomal regulation of signal transduction. The large amount of plasmalemmal PtdIns(4,5)P<sub>2</sub> plays a key role in stabilizing the active state of agonist-bound receptors and modulates formation of receptor– $\beta$ -arrestin complexes (69, 70). Conversely, the lack of PtdIns(4,5)P<sub>2</sub> in endosomal membranes may facilitate the disassembly of agonist–receptor– $\beta$ -arrestin complexes.

Compartment-specific characteristics of the ligand-receptor interaction can also distinguish endosomal β-arrestin binding from that in the plasma membrane. The relatively acidic environment of endosomes may accelerate ligand dissociation (71), and the consequently reduced receptor residence time can promote receptor resensitization (72). Moreover, the luminal ligand concentrations in different subcellular compartments may also differ from those in the extracellular space. Because of the relatively small volume of endosomes, ligand concentrations can be even greater. However, ligand depletion may also occur in endosomes, where endothelin-converting enzyme 1 and other peptidases can rapidly cleave peptide ligands, which prevents rebinding and thus reduces the signal transmission of intracellular receptors (73, 74). Considering that ligand binding can vary across different compartments, assessing how the endosomal microenvironment influences ligand-receptor interactions would be valuable. However, this represents a hitherto unaddressed technical challenge. To the best of our knowledge, there is no specific marker capable of selectively labeling the intraluminal site of early endosomes, which would enable the selective measurement of ligand binding kinetics within this compartment in live cells. Furthermore, because the kinetic constants that describe changes in endosomal pH or ligand concentrations are not precisely known, these were not incorporated into our mathematical model. Nevertheless, we speculate that including these mechanisms could further strengthen the conclusion of our study.

From a technical point of view, our findings refine the interpretation of various β-arrestin binding assay formats used in characterizing drug efficacy and biased signaling. Our experiments with a mutant β<sub>2</sub>AR revealed that commonly applied signal-amplification solutions that transform the receptor- $\beta$ -arrestin interaction type to class B, such as the C-terminal fusion of the cytoplasmic tail of V<sub>2</sub>R (75, 76), may not only enhance the extent of  $\beta$ -arrestin recruitment but artificially amplify differences between ligand efficacy values. We also resolved the previous conflict in data on the efficacy of OT at V<sub>2</sub>Rs in β-arrestin signaling. Its partial agonistic effect was identified through direct assessment of the BRET signal between the labeled receptor and  $\beta$ -arrestin2 (77), whereas its full agonistic effect was noted through an assay measuring the translocation of  $\beta$ -arrestin to the plasma membrane (78). We clarified this contradiction, showing that the number of V<sub>2</sub>R-β-arrestin complexes stimulated by OT was fewer than that stimulated by vasopressin within the endosomal compartment. Our computational data imply that the inhibition of receptor internalization may generally increase the detected  $\beta$ -arrestin signal of GPCRs with class B-type β-arrestin interactions. This insight offers a practical application: Inhibiting endocytosis during  $\beta$ -arrestin recruitment-based ligand screening may aid in identifying agonists even with high ligand dissociation rates.

To investigate the  $\beta$ -arrestin pathway in the context of biased signaling, BRET-based evaluation of the extent of receptor- $\beta$ -arrestin interactions in live cells is a key assay, because it reflects direct transducer coupling and thus readily provides data for the calculation of overall bias. However, experiments with and without the inhibition of receptor endocytosis could provide complementary information about the mechanism of drug action and help to separate the extent of ligand bias from other spatiotemporal factors that influence the pathway-specific efficacy of agonists.

We believe that our results can greatly assist the development of biased pharmaceutical compounds by improving our understanding of the molecular link between ligand characteristics and functional selectivity. A direct implication of this study is that increased endosomal  $\beta$ -arrestin recruitment is expected from ligands with long residence time at the receptor, and total  $\beta$ -arrestin recruitment can be enhanced by strategies that interfere with receptor internalization. Furthermore, our data propose that structure-activity relationship studies may benefit from the conduction of cell-based signaling assays both with and without the inhibition of receptor endocytosis and thus facilitate the rational design of drugs with compartment- and pathway-specific effects.

#### **MATERIALS AND METHODS**

#### Compounds

TRV 120023, TRV 120027, TRV 120055, TRV 120056 (24), and TAMRA-AngII were synthesized by Proteogenix. SII-AngII was obtained from Bachem. YM was purchased from Wako Chemicals. Candesartan, formoterol, and PTX were from Tocris. Rapamycin was bought from Selleckchem. Prolume Purple was obtained from Nano-Light. Coelenterazine h was purchased from Regis Technologies. All other reagents were from Sigma-Aldrich.

#### **Plasmid constructs**

Plasmids encoding the following constructs have been previously described: AT<sub>1</sub>R, AT<sub>1</sub>R-Rluc8, β<sub>2</sub>AR-3S-SLuc, β-arrestin2-K2A-Venus, Venus-Rab5 (here referred to as Venus-EE) (41), AT<sub>1</sub>R-Rluc (25), β-arrestin1–Venus, β-arrestin2–Venus (79), L10-Venus (here referred to as PM-Venus; Venus fused to "L10," the 10 first amino acid residues of mouse Lck protein, functioning as a myristoylatedpalmitoylated plasma membrane target sequence), L10-Cerulean (here referred to as PM-Cerulean), plasma membrane PtdIns(4,5) P<sub>2</sub> level BRET biosensor (L10-Venus-T2A-PLCδ1PH-SLuc) (37), GLuc-PM, NanoLuc-PM (44), V<sub>2</sub>R, super Renilla luciferase-tagged V<sub>2</sub>R (V<sub>2</sub>R-SLuc) (80), and β<sub>2</sub>AR-SLuc (33). PM-NanoLuc and EE-NanoLuc were generated by polymerase chain reaction (PCR) amplification of the coding sequence of NanoLuc with or without the stop codon using NanoLuc-PM as a template and replacing the Venus-encoding sequence with those in PM-Venus and Venus-EE, respectively (in PM-NanoLuc, the L10 sequence represents the target signal, whereas Rab5 protein marks early endosomes for EE-NanoLuc). The PtdIns(4,5)P<sub>2</sub> depletion system L10-FRB-T2A-FKBP-5-ptase construct was generated by replacing the PM2encoding sequence with the L10 sequence by PCR amplification using the PM2-FRB-T2A-mRFP-FKBP-5-ptase as a template. The sequence encoding FKBP-5-ptase was fused in frame to the T2A sequence by replacing the sequence encoding mRFP-FKBP-5ptase. RGS-FYVE was custom-synthesized in gBlock gene fragment by Integrated DNA Technologies (IDT) and was inserted into

pEGFP-C1 vector by replacing the sequence encoding enhanced green fluorescent protein between the Age I and Sma I restriction sites. RGS-FYVE contains a FLAG epitope followed by sequence encoding the regulator of G protein signaling homology domain of bovine GRK2 ("RGS," residues 45 to 178) (81) in frame fused to the tandem repeat of the FYVE domain of human endofin (Q739-K806) (39, 82). The plasma membrane-targeted RGS construct (RGS-CAAX) was generated by replacing the sequence encoding Venus in Venus-H-Ras-CAAX (83) with the sequence encoding RGS through Age I and EcoR I restriction digestion. TRUPATH was a gift from B. Roth (Addgene kit no. 1000000163) (31). Plasmids encoding untagged β-arrestin2, GRK2, and hemagglutinin (HA)-dynamin2A-K44A (Dyn-K44A) were provided by S. S. Ferguson (Department of Physiology, University of Western Ontario, London, Ontario, Canada) and K. Nakayama (Department of Physiological Chemistry, Graduate School of Pharmaceutical Sciences, Kyoto University, Sakyo-ku, Kyoto 606-8501, Japan). The Venus-MEK1-FLAG and FLAG-ERK2-Venus constructs were gifts from A. Reményi (Institute of Organic Chemistry, HUN-REN Research Centre for Natural Sciences, Budapest, Hungary).

#### Cell culture and transfection

The generation of the human embryonic kidney (HEK) 293A  $\Delta$ Gsix  $(\Delta G\alpha_s/\Delta G\alpha_{olf}/\Delta G\alpha_q/\Delta G\alpha_{11}/\Delta G\alpha_{12}/\Delta G\alpha_{13})$  cell line and the parental cell line were described previously (45). HEK 293T (American Type Culture Collection, CRL-3216), HEK 293A parental cells, and HEK 293A ΔGsix cells were cultured in Dulbecco's modified Eagle's medium (DMEM) supplemented with 10% fetal bovine serum and 1% penicillin/streptomycin. Cell lines were not tested for contaminants. The cells were transfected with the calcium phosphate precipitation method (in suspension for Gluc BRET measurements or as adherent cells for confocal microscopy measurements) or with Lipofectamine 2000 (Invitrogen; transfection was performed in suspension, used for all other measurements) as previously described (41, 44). The plasmid DNA amounts used are shown in table S3. For BRET measurements, transfected cells were cultured on white 96well poly-L-lysine-coated plates. The BRET measurements with parental and ΔGsix HEK 293A cells were performed 48 hours after transfection, whereas, in all other cases, the experiments were performed 24 to 28 hours after transfection. Unless specified otherwise, HEK 293A ΔGsix cells were pretreated for 20 hours with PTX (100 ng/ ml) before measurements were made.

#### **BRET** measurements

BRET measurements were performed with Thermo Fisher Varioskan or Varioskan Lux multimode plate readers as previously described (41, 44). Twenty-four to 28 hours after the cells were transfected, the cell culture medium was replaced with a modified Krebs-Ringer solution [120 mM NaCl, 10 mM Na-Hepes, 10 mM glucose, 4.7 mM KCl, 1.2 mM CaCl<sub>2</sub>, and 0.7 mM MgSO<sub>4</sub> (pH 7.4)], including a washing step. The expression of fluorescent protein–tagged constructs was determined by fluorescence intensity measurements (emission at 535 nm with excitation at 510 nm for Venus and emission at 515 nm with excitation at 400 nm for GFP2 fluorescence). The luciferase substrates and filters used are summarized in table S4. The BRET measurements were performed at 37°C, except for the ligand-binding measurements, which were made at 27°C. For kinetic measurements, first the basal BRET ratios were determined after the addition of the BRET substrate, then the indicated ligands were added, and BRET

was followed continuously. Basal BRET ratios were subtracted, and agonist-induced BRET changes were calculated by subtracting the BRET ratio of vehicle-treated cells. Unless otherwise stated, data are presented as a percentage of the AngII-induced (100 nM or 10 μM) change in the BRET ratio (BRET response). Because the coexpression of an additional protein to the BRET pair might have affected the BRET ratio by altering the BRET donor/acceptor ratio, percentage expression was only used for the same expression conditions. Because pretreatment of cells with hypertonic sucrose altered luminescence intensities, thereby potentially altering the measured BRET ratio, percentage expression was used solely for the comparison of agonist effects between the sucrose-pretreated samples. However, no conclusion was drawn regarding the effect of sucrose on the amplitude of the BRET signal. We determined the relative differences in the AUC of kinetic response curves of various agonists by averaging post-treatment values. Plasma membrane PtdIns(4,5)P<sub>2</sub> depletion was induced in cells expressing the L10-FRB-T2A-FKBP-5-ptase construct, from which L10-FRB (FRB targeted to the plasma membrane by the fusion tag L10) and FKBP-5-ptase (FKBP-fused 5-ptase) are translated in equimolar amounts because of the T2A sequence. Treatment with rapamycin (300 nM) induced heterodimerization between FRB and FKBP; thus, FKBP-5-ptase was translocated to the plasma membrane where it could cleave PtdIns(4,5)P2 (33), a molecule necessary for clathrin-mediated receptor endocytosis. Competitive ligand binding measurements were performed in live cells as described previously (44). Cells were cotransfected with plasmids encoding AT<sub>1</sub>R, GLuc-PM, Dyn-K44A, and β-arrestin2. To investigate the receptor occupancy of TAMRA-AngII, cells were treated with increasing concentrations of TAMRA-AngII for 2 hours at room temperature. Nonspecific binding was assessed in cells cotreated with 10 μM candesartan, a high-affinity AT<sub>1</sub>R antagonist. Specific binding was determined by subtracting the nonspecific signal from the total signal. A two-site-specific binding curve was fitted to obtain the  $K_{D_{low}}$  and  $K_{D_{high}}$  values. Thereafter, the kinetic rate constants  $(k_{\text{off\_LR}} \text{ and } k_{\text{on\_LR}} \text{ values})$  of the interaction between TAMRA-AngII and AT<sub>1</sub>R were determined. To assess  $k_{\text{off LR}}$ , 1  $\mu$ M TAMRA-AngII was applied for 15 min; thereafter, TAMRA-AngII was washed out, and medium containing the BRET substrate and 10 μM candesartan (to prevent rebinding) was added. The BRET ratio at time zero was determined in cells that were retreated with TAMRA-AngII without candesartan. The data were normalized to the BRET ratio of cells that were not treated with AT<sub>1</sub>R ligands. The basal BRET ratios were not determined in these experiments. A two-phase decay curve was fitted, and the initial proportion of the high- and low-affinity binding was calculated and set on the basis of the previously fitted  $K_{\rm D\ high}$  and  $B_{\text{max\_high}}$  values. Because the high-affinity binding site is occupied mostly in the applied concentration, the  $k_{\text{off}\_LR}$  value of the highaffinity binding site was used in further calculations. In  $k_{\text{on LR}}$  measurements, after assessment of the basal BRET ratios, the cells were treated with 300 nM TAMRA-AngII with or without 10 µM candesartan. The candesartan cotreatment was applied to determine the nonspecific signal, which was subtracted from the total signal. A one-site association binding curve equation was used to calculate the  $k_{\rm on\ LR}$  value of TAMRA-AngII. The kinetic binding parameters of unlabeled AT<sub>1</sub>R ligands were assessed by following the BRET ratio change after simultaneous treatment of 1 µM TAMRA-AngII and increasing concentrations of the unlabeled ligands. For the calculation of the  $k_{\text{on\_LR}}$  and  $k_{\text{off\_LR}}$  values of unlabeled ligands, we applied certain simplifications because of the large number of variables. We

used a one-site binding model because, in the applied TAMRA-AngII concentration, mostly the high-affinity binding site was occupied (fig. S14B). In addition, we assumed that all agonist-bound receptors induced β-arrestin2 binding (ternary complexes) and ignored the ligand-occupied receptor state that is not coupled to βarrestin. Kinetic binding parameters were fitted with the Motulsky-Mahan (kinetics of competitive binding) equation (84). To assess the dissociation rate of β-arrestin2-Venus from AT<sub>1</sub>R-RLuc, AT<sub>1</sub>R-βarrestin2 binding was first induced by treating with agonist for 12 min. The agonists were applied in ~30× half-maximal effective concentrations. Thereafter, agonists were displaced by the addition of 10 μM candesartan. One-phase dissociation curves were fitted to calculate the dissociation rate constant of β-arrestin2-Venus from  $AT_1R$ -RLuc ( $k_{dis}$ ). To evaluate the effect of pretreatment with 100 nM YM for 40 min, we used a slightly modified protocol. During this protocol, agonist treatment involved applying either 10 µM AngII or 10 μM ST-AngII for 26 min, and 30 μM candesartan was added subsequently. For association kinetics measurements, the frequency of well readings was increased, and injectors were used to apply the agonists. The data were then analyzed by one-phase association curve fitting to calculate the observed association rate constants ( $k_{as}$ ).

#### **Confocal fluorescence microscopy**

For confocal microscopy imaging of fixed cells, cells were seeded on ibidi μ-Slide 8-well plates coated with poly-L-lysine on the day before transfection. To image live cells, cells were seeded on poly-L-lysine-coated glass cover plates. The adherent cells were cotransfected with plasmids encoding plasma membrane-targeted Cerulean (PM-Cerulean), unlabeled AT<sub>1</sub>R, and β-arrestin2-Venus. In fixed cell experiments, cells were treated with AT<sub>1</sub>R ligands for 30 min in a modified Krebs-Ringer solution at 37°C. Next, the cells were fixed with ice-cold 4% paraformaldehyde in phosphate-buffered saline (PBS) for 15 min. Thereafter, the cells were washed three times with PBS for 5 min at room temperature. For live-cell experiments, coverslips were placed into a chamber, the medium was replaced with modified Krebs-Ringer solution, and measurements were performed at 37°C. Fluorescence imaging was performed with a Zeiss LSM 710 confocal laser-scanning microscope with a 40× objective in tile scan mode (4  $\times$  4) using autofocusing with a 2- $\mu$ m offset from the well bottom. The investigator was not blinded during image acquisition.

#### Western blotting

HEK 293T cells were plated on poly-L-lysine-coated six-well plates and were transfected on the following day with plasmids encoding AT<sub>1</sub>R with Dyn-K44A or empty pcDNA3.1 vector (Mock). The day after transfection, the cells were serum-starved in 1% bovine serum albumin-supplemented DMEM for 2 hours. Thereafter, cells were treated with 100 nM AngII or vehicle for 20 min at 37°C. Sample preparation was performed similarly as described previously (41). To stop the reactions, the plates were immediately placed on ice, and each well was washed twice with ice-cold PBS. The cells were then collected with a scraper and transferred into SDS sample buffer supplemented with phosphatase inhibitors (50 mM β-glycerophosphate, 10 mM sodium fluoride, 2 mM sodium orthovanadate, and 1 mM sodium pyrophosphate) and cOmplete Protease Inhibitor mixture (Roche). Thereafter, the samples were briefly sonicated, boiled at 95°C for 15 min, and centrifuged at 14,000g at 4°C for 10 min. Subsequently, the proteins were resolved by SDS-polyacrylamide gel

electrophoresis and then transferred onto polyvinylidene difluoride membranes. The membranes were blocked with 5% (w/v) fat-free milk powder in PBS with 0.05% (v/v) Tween 20 (PBST) at room temperature for 1 hour. Membranes were incubated overnight at 4°C with primary antibodies diluted at 1:1000 in PBST with 5% fat-free milk. The applied primary antibodies were mouse anti-phospho-p44/42 MAPK (Thr<sup>202</sup> and Tyr<sup>204</sup>) antibody (product number 9106S, Cell Signaling Technology, RRID: AB\_331768) and rabbit anti-p44/42 MAPK (product number 9102S, Cell Signaling Technology, RRID: AB\_330744). After the membranes were washed three times with PBST for 10 min each, they were incubated with horseradish peroxidase (HRP)-conjugated anti-mouse (product number 7076S, Cell Signaling Technology, RRID: AB\_330924) or goat fluorescently labeled AzureSpectra 800 anti-rabbit (S1021, Azure Biosystems) secondary antibodies at a 1:5000 dilution in PBST with 5% fat-free milk for 1 hour at room temperature. The incubation was followed by another three washes. HRP-conjugated antibodies were visualized with Immobilon Western chemiluminescent HRP Substrate (Millipore). Chemiluminescence and fluorescence were detected with Azure 600 Western blot Imaging System (Azure Biosystems). After the initial development, the membranes were treated with a guanidine hydrochloride-based solution [20 mM tris-HCl, 6 M guanidine hydrochloride, 0.2% Nonidet P-40, and 0.1 M β-mercaptoethanol (pH 7.5)] and then incubated with other antibodies, using the same protocol as that for the anti-MAPK antibodies. First, rabbit anti-HA (SAB4300603, Sigma-Aldrich, RRID: AB\_10620829, diluted at 1:1000) primary antibody labeling was developed with chemiluminescence detection after incubation with HRP-conjugated goat anti-rabbit antibody (7074S, Cell Signaling Technology, RRID: AB\_2099233). Thereafter, incubation with mouse anti-glyceraldehyde-3-phosphate dehydrogenase (GAPDH; product number 5174S, Cell Signaling Technology, RRID: AB\_10622025, diluted at 1:1000) was performed, followed by incubation with HRP-conjugated anti-mouse secondary antibody. Subsequent detection of chemiluminescence at the expected molecular weight confirmed the presence of GAPDH, which served as the loading control.

#### **Image analysis**

Analysis of confocal microscopy images was performed with Python. The cells were detected with the Cellpose library (85) in the PM-Cerulean channel. The puncta were detected with the TensorFlow implementation of the Pix2Pix model (86, 87) trained on manually labeled images from the experiments. Further analysis of the cell and puncta masks aligned with the original images was performed with the Pandas library (88).  $\beta$ -Arrestin2–Venus abundances were slightly different in the parental and the  $\Delta Gsix$  HEK 293A cells. Therefore, in the experiments in which both cell lines were used, only the cells in the pixel intensity range present in both samples (250 to 600) were used. The Python code used in the analysis can be found at Zenodo (https://zenodo.org/records/10072720, DOI: 10.5281/zenodo.10072720). Densitometric analysis of Western blots was performed with Fiji ImageJ software.

#### **Mathematical modeling**

We developed a mathematical model of GPCR signaling that captures the effects of various factors on receptor– $\beta$ -arrestin binding. The model is based on ODEs and comprises 43 molecular species and 96 reactions, such as enzymatic reactions, binding events, and compartment changes. The molecular concentrations and reaction rate

constants of the model (tables S1 and S2, respectively) were obtained from literature sources. The time derivatives of the molecular concentrations were calculated with the reaction equations (table S2) and were integrated numerically. Initial parameters of the ODE model, in the absence of ligand stimulation, represent a steady state. Our model is composed of four basic modules: receptor- $\beta$ -arrestin interactions, heterotrimeric G protein interactions, PLC activation, and second messenger generation (fig. S19). In addition, the model considers three compartments: the plasma membrane, the cytosol, and intracellular vesicles. The receptor–β-arrestin module incorporates ligand binding to receptors, receptor activation and deactivation, receptor phosphorylation and dephosphorylation, β-arrestin binding, and receptor internalization (fig. S19A). Note that internalized receptors can maintain ligand and β-arrestin binding. We modeled receptor internalization as a unidirectional reaction and did not include receptor recycling or degradation in the model. Note that the phosphorylation rate of intracellular receptors was set as 100 times less than that of plasma-membrane receptors. We also incorporated the rational assumption that the agonist-activated, phosphorylated receptor exhibits a higher affinity for  $\beta$ -arrestin compared with that of its inactive, phosphorylated counterpart. Because our simulation is tailored to the  $G_{q/11}$  protein–coupled  $AT_1$  angiotensin receptor, the G protein and PLC modules of our model reflect the signaling of G<sub>q/11</sub> heterotrimeric G proteins, including the receptor–G protein interaction, G protein dissociation and reassociation (fig. S19B), and the interaction between the G protein  $\alpha$  subunit and PLC (fig. S19C). In addition, our second messenger module incorporates PtdIns(4,5)P<sub>2</sub> synthesis and PLC-induced cleavage of PtdIns(4,5) P<sub>2</sub> into diacylglycerol and inositol 1,4,5-trisphosphate (fig. S19D). We used three different sets of initial values in the simulations: one resembling a receptor per  $\beta$ -arrestin-overexpression system ([receptor] = 5000 molecules per  $\mu m^2$ , [arrestin] = 15,000 molecules per  $\mu m^2$ , and [G protein] = 40 molecules per  $\mu$ m<sup>2</sup>); another resembling a receptor/G protein overexpression system ([receptor] = 5000 molecules per  $\mu m^2$ , [arrestin] = 1000 molecules per  $\mu m^2$ , and [G protein] = 4000 molecules per  $\mu$ m<sup>2</sup>), and another resembling a receptor overexpression system ([receptor] = 5000 molecules per  $\mu$ m<sup>2</sup>, [arrestin] = 1000 molecules per  $\mu$ m<sup>2</sup>, and [G protein] = 40 molecules per μm<sup>2</sup>). These systems correspond to typical experimental systems for measuring β-arrestin and G protein activation or second messenger generation, respectively. We used Python 3.8 to run the simulations and for data analysis. The Scipy library (89) was used for numerical integration. The code to reproduce our results is available at Zenodo (https://zenodo.org/records/10091027, DOI: 10.5281/zenodo.10091027).

#### Statistical analysis

Figures showing experimental data were generated with GraphPad Prism 9 software. Unless otherwise stated, this software was also used for statistical analysis, and the name of each analysis is indicated in this paragraph. "Log(agonist) vs. response – Variable slope (four parameters)" nonlinear regression curves were fitted on the concentration-response data. The bottom was constrained to 0, and the Hill slope was set to 1 for  $\beta$ -arrestin2 binding and the  $G_q$  TRUPATH biosensor data. Unpaired, two-tailed t tests were used to compare the means of two distributions. Variances of distributions were analyzed with Levene's tests using Microsoft Excel 365; analyses were conducted on datasets scaled relative to their averages. Multiple groups, based on the experimental setting, were analyzed by one-way analysis of

variance (ANOVA), two-way ANOVA, repeated-measures two-way ANOVA, or three-way ANOVA. A Bonferroni post hoc test was used if multiple comparisons were performed. Unless otherwise stated, kinetic data were normalized to baseline (data points before stimulation). Timescales were adjusted to better indicate the time length between stimulation and the first stimulated measurement point. The data of time point zero represent the data of the last time point before stimulation. The time of one cycle length was subtracted from the time between the last baseline point and the first stimulated points and was added to the time between the last two baseline points. When distributions of agonist-induced  $\beta$ -arrestin2–Venus puncta in each identified cell were analyzed, outliers were identified and excluded with the ROUT method (Q = 1%). The  $k_{\text{off LR}}$  and  $k_{\text{on LR}}$  values for TAMRA-AngII were calculated with the association kinetics (one ligand concentration) and dissociation kinetics equations, respectively. The  $k_{\text{off}\_LR}$  and  $k_{\text{on}\_LR}$  values for unlabeled agonists were calculated by the "kinetics of competitive binding" equation (84). The  $k_{as}$ and  $k_{dis}$  values of the AT<sub>1</sub>R–RLuc– $\beta$ -arrestin2–Venus interaction were determined by nonlinear regression curve fitting using "one-phase association" and "one-phase decay" equations, respectively. The operational model (35) was applied to calculate the bias factor  $[\Delta \Delta \log(\tau/K_A)]$ or LogBias (36); equation 2 as described by Herenbrink et al. (18) was applied]. Time-dependent changes in the LogBias factor were analyzed by fitting the LogBias ~ ligand \* time linear model. The linear model was fitted with the statsmodels (90) Python library. The P values for the ligand: time interaction term were reported, corrected by the Holm-Šidák method. Data are means ± SEM. All experiments were independently performed at least three times, and N in the figure legends always indicates the number of independent biological replicates. BRET measurements were made in duplicate or triplicate, with the exception of MEK1 and ERK2 complex formation BRET assays, where sextuplicates were used.

#### **Supplementary Materials**

This PDF file includes:

Figs. S1 to S21 Table S4

#### Other Supplementary Material for this manuscript includes the following:

Tables S1 to S3 MDAR Reproducibility Checklist

#### **REFERENCES AND NOTES**

- P. Kolb, T. Kenakin, S. P. H. Alexander, M. Bermudez, L. M. Bohn, C. S. Breinholt, M. Bouvier, S. J. Hill, E. Kostenis, K. A. Martemyanov, R. R. Neubig, H. O. Onaran, S. Rajagopal, B. L. Roth, J. Selent, A. K. Shukla, M. E. Sommer, D. E. Gloriam, Community guidelines for GPCR ligand bias: IUPHAR review 32. Br. J. Pharmacol. 179, 3651–3674 (2022).
- A. C. Holloway, H. Qian, L. Pipolo, J. Ziogas, S. Miura, S. Karnik, B. R. Southwell, M. J. Lew, W. G. Thomas, Side-chain substitutions within angiotensin II reveal different requirements for signaling, internalization, and phosphorylation of type 1A angiotensin receptors. Mol. Pharmacol. 61, 768–777 (2002).
- H. Wei, S. Ahn, S. K. Shenoy, S. S. Karnik, L. Hunyady, L. M. Luttrell, R. J. Lefkowitz, Independent β-arrestin 2 and G protein-mediated pathways for angiotensin II activation of extracellular signal-regulated kinases 1 and 2. Proc. Natl. Acad. Sci. U.S.A. 100, 10782–10787 (2003).
- A. Saulière, M. Bellot, H. Paris, C. Denis, F. Finana, J. T. Hansen, M.-F. Altié, M.-H. Seguelas, A. Pathak, J. L. Hansen, J.-M. Sénard, C. Galés, Deciphering biased-agonism complexity reveals a new active AT1 receptor entity. *Nat. Chem. Biol.* 8, 622–630 (2012).
- B. Zimmerman, A. Beautrait, B. Aguila, R. Charles, E. Escher, A. Claing, M. Bouvier,
   S. A. Laporte, Differential β-arrestin-dependent conformational signaling and cellular responses revealed by angiotensin analogs. Sci. Signal. 5, ra33 (2012).
- Y. Namkung, C. LeGouill, S. Kumar, Y. Cao, L. B. Teixeira, V. Lukasheva, J. Giubilaro,
   S. C. Simões, J.-M. Longpré, D. Devost, T. E. Hébert, G. Piñeyro, R. Leduc, C. M. Costa-Neto,

- M. Bouvier, S. A. Laporte, Functional selectivity profiling of the angiotensin II type 1 receptor using pathway-wide BRET signaling sensors. *Sci. Signal.* **11**, eaat1631 (2018).
- K. Kawakami, M. Yanagawa, S. Hiratsuka, M. Yoshida, Y. Ono, M. Hiroshima, M. Ueda,
  J. Aoki, Y. Sako, A. Inoue, Heterotrimeric Gq proteins act as a switch for GRK5/6 selectivity
  underlying β-arrestin transducer bias. Nat. Commun. 13, 487 (2022).
- G. Boerrigter, D. G. Soergel, J. D. Violin, M. W. Lark, J. C. Burnett Jr., TRV120027, a novel β-arrestin biased ligand at the angiotensin II type I receptor, unloads the heart and maintains renal function when added to furosemide in experimental heart failure. Circ. Heart Fail. 5, 627–634 (2012).
- D. M. Ryba, J. Li, C. L. Cowan, B. Russell, B. M. Wolska, R. J. Solaro, Long-term biased β-arrestin signaling improves cardiac structure and function in dilated cardiomyopathy. *Circulation* 135, 1056–1070 (2017).
- L. B. Teixeira, L. T. Parreiras-e-Silva, T. Bruder-Nascimento, D. A. Duarte, S. C. Simões, R. M. Costa, D. Y. Rodríguez, P. A. B. Ferreira, C. A. A. Silva, E. P. Abrao, E. B. Oliveira, M. Bouvier, R. C. Tostes, C. M. Costa-Neto, Ang-(1-7) is an endogenous β-arrestin-biased agonist of the AT1 receptor with protective action in cardiac hypertrophy. Sci. Rep. 7, 11903 (2017).
- J. D. Violin, S. M. DeWire, D. Yamashita, D. H. Rominger, L. Nguyen, K. Schiller, E. J. Whalen, M. Gowen, M. W. Lark, Selectively engaging β-arrestins at the angiotensin II type 1 receptor reduces blood pressure and increases cardiac performance. *J. Pharmacol. Exp. Ther.* 335, 572–579 (2010).
- Z. P. Jara, T. J. Harford, K. D. Singh, R. Desnoyer, A. Kumar, D. Srinivasan, S. S. Karnik, Distinct mechanisms of β-arrestin-biased agonist and blocker of AT1R in preventing aortic aneurysm and associated mortality. Hypertension 80, 385–402 (2023).
- D. Devost, R. Sleno, D. Pétrin, A. Zhang, Y. Shinjo, R. Okde, J. Aoki, A. Inoue, T. E. Hébert, Conformational profiling of the AT1 angiotensin II receptor reflects biased agonism, G protein coupling, and cellular context. J. Biol. Chem. 292, 5443–5456 (2017).
- L. M. Wingler, M. Elgeti, D. Hilger, N. R. Latorraca, M. T. Lerch, D. P. Staus, R. O. Dror, B. K. Kobilka, W. L. Hubbell, R. J. Lefkowitz, Angiotensin analogs with divergent bias stabilize distinct receptor conformations. *Cell* 176, 468–478.e11 (2019).
- L. M. Wingler, M. A. Skiba, C. McMahon, D. P. Staus, A. L. W. Kleinhenz, C.-M. Suomivuori, N. R. Latorraca, R. O. Dror, R. J. Lefkowitz, A. C. Kruse, Angiotensin and biased analogs induce structurally distinct active conformations within a GPCR. Science 367, 888–892 (2020).
- J. R. Lane, L. T. May, R. G. Parton, P. M. Sexton, A. Christopoulos, A kinetic view of GPCR allostery and biased agonism. Nat. Chem. Biol. 13, 929–937 (2017).
- M. Grundmann, E. Kostenis, Temporal bias: Time-encoded dynamic GPCR signaling. Trends Pharmacol. Sci. 38, 1110–1124 (2017).
- C. Klein Herenbrink, D. A. Sykes, P. Donthamsetti, M. Canals, T. Coudrat, J. Shonberg,
   P. J. Scammells, B. Capuano, P. M. Sexton, S. J. Charlton, J. A. Javitch, A. Christopoulos,
   J. R. Lane, The role of kinetic context in apparent biased agonism at GPCRs. *Nat. Commun.* 7, 10842 (2016).
- D. Wacker, S. Wang, J. D. McCorvy, R. M. Betz, A. J. Venkatakrishnan, A. Levit, K. Lansu, Z. L. Schools, T. Che, D. E. Nichols, B. K. Shoichet, R. O. Dror, B. L. Roth, Crystal structure of an LSD-bound human serotonin receptor. *Cell* 168, 377–389.e12 (2017).
- R. Irannejad, V. Pessino, D. Mika, B. Huang, P. B. Wedegaertner, M. Conti, M. von Zastrow, Functional selectivity of GPCR-directed drug action through location bias. *Nat. Chem. Biol.* 13, 799–806 (2017).
- M. Stoeber, D. Jullié, B. T. Lobingier, T. Laeremans, J. Steyaert, P. W. Schiller, A. Manglik, M. von Zastrow, A genetically encoded biosensor reveals location bias of opioid drug action. *Neuron* 98, 963–976.e5 (2018).
- A. D. White, K. A. Peña, L. J. Clark, C. S. Maria, S. Liu, F. G. Jean-Alphonse, J. Y. Lee, S. Lei, Z. Cheng, C.-L. Tu, F. Fang, N. Szeto, T. J. Gardella, K. Xiao, S. H. Gellman, I. Bahar, I. Sutkeviciute, W. Chang, J.-P. Vilardaga, Spatial bias in cAMP generation determines biological responses to PTH type 1 receptor activation. Sci. Signal. 14, eabc5944 (2021).
- D. S. Eiger, N. Boldizsar, C. C. Honeycutt, J. Gardner, S. Kirchner, C. Hicks, I. Choi, U. Pham, K. Zheng, A. Warman, J. S. Smith, J. Y. Zhang, S. Rajagopal, Location bias contributes to functionally selective responses of biased CXCR3 agonists. *Nat. Commun.* 13, 5846 (2022).
- S. Rajagopal, S. Ahn, D. H. Rominger, W. Gowen-MacDonald, C. M. Lam, S. M. DeWire, J. D. Violin, R. J. Lefkowitz, Quantifying ligand bias at seven-transmembrane receptors. *Mol. Pharmacol.* 80, 367–377 (2011).
- G. Szakadáti, A. D. Tóth, I. Oláh, L. S. Erdélyi, T. Balla, P. Várnai, L. Hunyady, A. Balla, Investigation of the fate of type I angiotensin receptor after biased activation. *Mol. Pharmacol.* 87, 972–981 (2015).
- R. T. Strachan, J. Sun, D. H. Rominger, J. D. Violin, S. Ahn, A. R. B. Thomsen, X. Zhu, A. Kleist, T. Costa, R. J. Lefkowitz, Divergent transducer-specific molecular efficacies generate biased agonism at a G protein-coupled receptor (GPCR). J. Biol. Chem. 289, 14211–14224 (2014).
- S. Angers, A. Salahpour, E. Joly, S. Hilairet, D. Chelsky, M. Dennis, M. Bouvier, Detection of β<sub>2</sub>-adrenergic receptor dimerization in living cells using bioluminescence resonance energy transfer (BRFT). *Proc. Natl. Acad. Sci. U.S.A.* 97, 3684–3689 (2000).
- C. Galés, R. V. Rebois, M. Hogue, P. Trieu, A. Breit, T. E. Hébert, M. Bouvier, Real-time monitoring of receptor and G-protein interactions in living cells. *Nat. Methods* 2, 177–184 (2005).

- C. Galés, J. J. J. Van Durm, S. Schaak, S. Pontier, Y. Percherancier, M. Audet, H. Paris, M. Bouvier, Probing the activation-promoted structural rearrangements in preassembled receptor–G protein complexes. *Nat. Struct. Mol. Biol.* 13, 778–786 (2006).
- S. C. Wright, M. Bouvier, Illuminating the complexity of GPCR pathway selectivity

   Advances in biosensor development. Curr. Opin. Struct. Biol. 69, 142–149 (2021).
- R. H. J. Olsen, J. F. DiBerto, J. G. English, A. M. Glaudin, B. E. Krumm, S. T. Slocum, T. Che, A. C. Gavin, J. D. McCorvy, B. L. Roth, R. T. Strachan, TRUPATH, an open-source biosensor platform for interrogating the GPCR transducerome. *Nat. Chem. Biol.* 16, 841–849 (2020).
- Z. Gáborik, M. Szaszák, L. Szidonya, B. Balla, S. Paku, K. J. Catt, A. J. Clark, L. Hunyady, Beta-arrestin- and dynamin-dependent endocytosis of the AT1 angiotensin receptor. *Mol. Pharmacol.* 59, 239–247 (2001).
- D. J. Tóth, J. T. Tóth, G. Gulyás, A. Balla, T. Balla, L. Hunyady, P. Várnai, Acute depletion of plasma membrane phosphatidylinositol 4,5-bisphosphate impairs specific steps in endocytosis of the G-protein-coupled receptor. J. Cell Sci. 125, 2185–2197 (2012).
- J. E. Heuser, R. G. Anderson, Hypertonic media inhibit receptor-mediated endocytosis by blocking clathrin-coated pit formation. J. Cell Biol. 108, 389–400 (1989).
- J. W. Black, P. Leff, Operational models of pharmacological agonism. Proc. R. Soc. Lond. B Biol. Sci. 220, 141–162 (1983).
- T. Kenakin, C. Watson, V. Muniz-Medina, A. Christopoulos, S. Novick, A simple method for quantifying functional selectivity and agonist bias. ACS Chem. Nerosci. 3, 193–203 (2012).
- J. T. Tóth, G. Gulyás, D. J. Tóth, A. Balla, G. R. V. Hammond, L. Hunyady, T. Balla, P. Várnai, BRET-monitoring of the dynamic changes of inositol lipid pools in living cells reveals a PKC-dependent PtdIns4P increase upon EGF and M3 receptor activation. *Biochim. Biophys. Acta* 1861, 177–187 (2016).
- C. C. Clayton, P. Donthamsetti, N. A. Lambert, J. A. Javitch, K. A. Neve, Mutation of three residues in the third intracellular loop of the dopamine D2 receptor creates an internalization-defective receptor. J. Biol. Chem. 289, 33663–33675 (2014).
- Y. Namkung, C. Le Gouill, V. Lukashova, H. Kobayashi, M. Hogue, E. Khoury, M. Song, M. Bouvier, S. A. Laporte, Monitoring G protein-coupled receptor and β-arrestin trafficking in live cells using enhanced bystander BRET. *Nat. Commun.* 7, 12178 (2016).
- S. Ahn, S. K. Shenoy, H. Wei, R. J. Lefkowitz, Differential kinetic and spatial patterns of β-arrestin and G protein-mediated ERK activation by the angiotensin II receptor. J. Biol. Chem. 279, 35518–35525 (2004).
- A. D. Tóth, S. Prokop, P. Gyombolai, P. Várnai, A. Balla, V. V. Gurevich, L. Hunyady, G. Turu, Heterologous phosphorylation–induced formation of a stability lock permits regulation of inactive receptors by β-arrestins. J. Biol. Chem. 293, 876–892 (2018).
- L. M. Luttrell, F. L. Roudabush, E. W. Choy, W. E. Miller, M. E. Field, K. L. Pierce,
   R. J. Lefkowitz, Activation and targeting of extracellular signal-regulated kinases by beta-arrestin scaffolds. *Proc. Natl. Acad. Sci. U.S.A.* 98, 2449–2454 (2001).
- 43. L. Zhou, X. Chen, Y. Gu, J. Liang, Transport characteristics of candesartan in human intestinal Caco-2 cell line. *Biopharm. Drug Dispos.* **30**, 259–264 (2009).
- A. D. Tóth, D. Garger, S. Prokop, E. Soltész-Katona, P. Várnai, A. Balla, G. Turu, L. Hunyady, A general method for quantifying ligand binding to unmodified receptors using *Gaussia* luciferase. *J. Biol. Chem.* 296, 100366 (2021).
- M. Grundmann, N. Merten, D. Malfacini, A. Inoue, P. Preis, K. Simon, N. Rüttiger, N. Ziegler, T. Benkel, N. K. Schmitt, S. Ishida, I. Müller, R. Reher, K. Kawakami, A. Inoue, U. Rick, T. Kühl, D. Imhof, J. Aoki, G. M. König, C. Hoffmann, J. Gomeza, J. Wess, E. Kostenis, Lack of beta-arrestin signaling in the absence of active G proteins. Nat. Commun. 9, 341 (2018).
- X.-F. Xiong, H. Zhang, C. R. Underwood, K. Harpsøe, T. J. Gardella, M. F. Wöldike, M. Mannstadt, D. E. Gloriam, H. Bräuner-Osborne, K. Strømgaard, Total synthesis and structure–activity relationship studies of a series of selective G protein inhibitors. *Nat. Chem.* 8, 1035–1041 (2016).
- S. C. Wright, V. Lukasheva, C. Le Gouill, H. Kobayashi, B. Breton, S. Mailhot-Larouche, É. Blondel-Tepaz, N. Antunes Vieira, C. Costa-Neto, M. Héroux, N. A. Lambert, L. T. Parreiras-e-Silva, M. Bouvier, BRET-based effector membrane translocation assay monitors GPCR-promoted and endocytosis-mediated G<sub>q</sub> activation at early endosomes. *Proc. Natl. Acad. Sci. U.S.A.* 118, e2025846118 (2021).
- J. D. Violin, S. M. DeWire, W. G. Barnes, R. J. Lefkowitz, G protein-coupled receptor kinase and β-arrestin-mediated desensitization of the angiotensin II type 1A receptor elucidated by diacylglycerol dynamics. *J. Biol. Chem.* 281, 36411–36419 (2006).
- C. D. Nelson, J. J. Kovacs, K. N. Nobles, E. J. Whalen, R. J. Lefkowitz, β-arrestin scaffolding of phosphatidylinositol 4-phosphate 5-kinase Iα promotes agoniststimulated sequestration of the β2-adrenergic receptor. J. Biol. Chem. 283, 21003–21101 (2008)
- R. H. Oakley, S. A. Laporte, J. A. Holt, M. G. Caron, L. S. Barak, Differential affinities of visual arrestin, βarrestin1, and βarrestin2 for G protein-coupled receptors delineate two major classes of receptors. J. Biol. Chem. 275, 17201–17210 (2000).
- D. Zindel, A. J. Butcher, S. Al-Sabah, P. Lanzerstorfer, J. Weghuber, A. B. Tobin, M. Bünemann, C. Krasel, Engineered hyperphosphorylation of the β<sub>2</sub>-adrenoceptor prolongs arrestin-3 binding and induces arrestin internalization. *Mol. Pharmacol.* 87, 349–362 (2015).

- S. J. Vayttaden, J. Friedman, T. M. Tran, T. C. Rich, C. W. Dessauer, R. B. Clark, Quantitative modeling of GRK-mediated β2AR regulation. *PLOS Comput. Biol.* 6, e1000647 (2010).
- S.-R. Jung, J. B. Seo, Y. Deng, C. L. Asbury, B. Hille, D.-S. Koh, Contributions of protein kinases and β-arrestin to termination of protease-activated receptor 2 signaling. J. Gen. Physiol. 147, 255–271 (2016).
- D. Heitzler, G. Durand, N. Gallay, A. Rizk, S. Ahn, J. Kim, J. D. Violin, L. Dupuy, C. Gauthier,
   V. Piketty, P. Crépieux, A. Poupon, F. Clément, F. Fages, R. J. Lefkowitz, E. Reiter, Competing
   G protein-coupled receptor kinases balance G protein and β-arrestin signaling. Mol. Syst. Biol. 8, 590 (2012).
- B. H. Falkenburger, J. B. Jensen, B. Hille, Kinetics of M1 muscarinic receptor and G protein signaling to phospholipase C in living cells. J. Gen. Physiol. 135, 81–97 (2010).
- B. H. Falkenburger, E. J. Dickson, B. Hille, Quantitative properties and receptor reserve of the DAG and PKC branch of Gq-coupled receptor signaling. J. Gen. Physiol. 141, 537–555 (2013).
- V. Iyer, T. M. Tran, E. Foster, W. Dai, R. B. Clark, B. J. Knoll, Differential phosphorylation and dephosphorylation of β<sub>2</sub>-adrenoceptor sites Ser262 and Ser355,356. *Br. J. Pharmacol.* 147, 249–259 (2006)
- D. R. Sibley, R. H. Strasser, J. L. Benovic, K. Daniel, R. J. Lefkowitz, Phosphorylation/ dephosphorylation of the beta-adrenergic receptor regulates its functional coupling to adenylate cyclase and subcellular distribution. *Proc. Natl. Acad. Sci. U.S.A.* 83, 9408–9412 (1986).
- S. Pippig, S. Andexinger, M. J. Lohse, Sequestration and recycling of beta 2-adrenergic receptors permit receptor resensitization. *Mol. Pharmacol.* 47, 666–676 (1995).
- K. M. Krueger, Y. Daaka, J. A. Pitcher, R. J. Lefkowitz, The role of sequestration in G protein-coupled receptor resensitization. J. Biol. Chem. 272, 5–8 (1997).
- B. Jones, T. Buenaventura, N. Kanda, P. Chabosseau, B. M. Owen, R. Scott, R. Goldin, N. Angkathunyakul, I. R. Corrêa Jr., D. Bosco, P. R. Johnson, L. Piemonti, P. Marchetti, A. M. J. Shapiro, B. J. Cochran, A. C. Hanyaloglu, A. Inoue, T. Tan, G. A. Rutter, A. Tomas, S. R. Bloom, Targeting GLP-1 receptor trafficking to improve agonist efficacy. *Nat. Commun.* 9, 1602 (2018).
- E. M. Bech, A. Kaiser, K. Bellmann-Sickert, S. S.-R. Nielsen, K. K. Sørensen, L. Elster,
   N. Hatzakis, S. L. Pedersen, A. G. Beck-Sickinger, K. J. Jensen, Half-life extending modifications of peptide YY<sub>3-36</sub> direct receptor-mediated internalization. *Mol. Pharm.* 16, 3665–3677 (2019).
- N. Mösslein, L. G. Pohle, A. Fuss, M. Bünemann, C. Krasel, Residency time of agonists does not affect the stability of GPCR-arrestin complexes. Br. J. Pharmacol. 179, 4107–4116 (2022).
- V. V. Gurevich, E. V. Gurevich, GPCR signaling regulation: The role of GRKs and arrestins. Front. Pharmacol. 10. 125 (2019).
- 65. K. N. Nobles, K. Xiao, S. Ahn, A. K. Shukla, C. M. Lam, S. Rajagopal, R. T. Strachan, T.-Y. Huang, E. A. Bressler, M. R. Hara, S. K. Shenoy, S. P. Gygi, R. J. Lefkowitz, Distinct phosphorylation sites on the  $\beta_2$ -adrenergic receptor establish a barcode that encodes differential functions of  $\beta$ -arrestin. *Sci. Signal.* **4**, ra51 (2011).
- M.-H. Lee, K. M. Appleton, E. G. Strungs, J. Y. Kwon, T. A. Morinelli, Y. K. Peterson,
   A. Laporte, L. M. Luttrell, The conformational signature of β-arrestin2 predicts its trafficking and signalling functions. *Nature* 531, 665–668 (2016).
- A. K. Shukla, J. D. Violin, E. J. Whalen, D. Gesty-Palmer, S. K. Shenoy, R. J. Lefkowitz, Distinct conformational changes in β-arrestin report biased agonism at seven-transmembrane receptors. *Proc. Natl. Acad. Sci. U.S.A.* 105, 9988–9993 (2008).
- J. Gardner, D. S. Eiger, C. Hicks, I. Choi, U. Pham, A. Chundi, O. Namjoshi, S. Rajagopal, GPCR kinases differentially modulate biased signaling downstream of CXCR3 depending on their subcellular localization. Sci. Signal. 17, eadd9139 (2024).
- J. Janetzko, R. Kise, B. Barsi-Rhyne, D. H. Siepe, F. M. Heydenreich, K. Kawakami, M. Masureel, S. Maeda, K. C. Garcia, M. von Zastrow, A. Inoue, B. K. Kobilka, Membrane phosphoinositides regulate GPCR-β-arrestin complex assembly and dynamics. *Cell* 185, 4560–4573.e19 (2022).
- H.-Y. Yen, K. K. Hoi, I. Liko, G. Hedger, M. R. Horrell, W. Song, D. Wu, P. Heine, T. Warne, Y. Lee, B. Carpenter, A. Plückthun, C. G. Tate, M. S. P. Sansom, C. V. Robinson, Ptdlns(4,5)P2 stabilizes active states of GPCRs and enhances selectivity of G-protein coupling. *Nature* 559, 423–427 (2018).
- L. Hunyady, A. J. Baukal, Z. Gáborik, J. A. Olivares-Reyes, M. Bor, M. Szaszák, R. Lodge, K. J. Catt, T. Balla, Differential PI 3-kinase dependence of early and late phases of recycling of the internalized AT1 angiotensin receptor. *J. Cell Biol.* 157, 1211–1222 (2002).
- D. A. Duarte, L. T. Parreiras-e-Silva, E. B. Oliveira, M. Bouvier, C. M. Costa-Neto, Angiotensin Il type 1 receptor tachyphylaxis is defined by agonist residence time. *Hypertension* 79, 115–125 (2022).
- B. E. Padilla, G. S. Cottrell, D. Roosterman, S. Pikios, L. Muller, M. Steinhoff, N. W. Bunnett, Endothelin-converting enzyme-1 regulates endosomal sorting of calcitonin receptor-like receptor and β-arrestins. J. Cell Biol. 179, 981–997 (2007).
- D. Roosterman, G. S. Cottrell, B. E. Padilla, L. Muller, C. B. Eckman, N. W. Bunnett,
   M. Steinhoff, Endothelin-converting enzyme 1 degrades neuropeptides in endosomes to control receptor recycling. *Proc. Natl. Acad. Sci. U.S.A.* 104, 11838–11843 (2007).
- W. K. Kroeze, M. F. Sassano, X.-P. Huang, K. Lansu, J. D. McCorvy, P. M. Giguère, N. Sciaky, B. L. Roth, PRESTO-Tango as an open-source resource for interrogation of the druggable human GPCRome. *Nat. Struct. Mol. Biol.* 22, 362–369 (2015).

- R. H. Oakley, S. A. Laporte, J. A. Holt, L. S. Barak, M. G. Caron, Association of β-arrestin with G protein-coupled receptors during clathrin-mediated endocytosis dictates the profile of receptor resensitization. *J. Biol. Chem.* 274, 32248–32257 (1999).
- M.-C. Frantz, L. P. Pellissier, E. Pflimlin, S. Loison, J. Gandía, C. Marsol, T. Durroux,
   B. Mouillac, J. A. J. Becker, J. Le Merrer, C. Valencia, P. Villa, D. Bonnet, M. Hibert, LIT-001,
   the first nonpeptide oxytocin receptor agonist that improves social interaction in a mouse model of autism. J. Med. Chem. 61, 8670–8692 (2018).
- F. M. Heydenreich, B. Plouffe, A. Rizk, D. Milić, J. Zhou, B. Breton, C. Le Gouill, A. Inoue, M. Bouvier, D. B. Veprintsev, Michaelis-menten quantification of ligand signaling bias applied to the promiscuous vasopressin V2 receptor. Mol. Pharmacol. 102, 139–149 (2022).
- P. Gyombolai, A. D. Tóth, D. Tímár, G. Turu, L. Hunyady, Mutations in the 'DRY' motif of the CB1 cannabinoid receptor result in biased receptor variants. J. Mol. Endocrinol. 54, 75–89 (2015).
- L. S. Erdélyi, A. Balla, A. Patócs, M. Tóth, P. Várnai, L. Hunyady, Altered agonist sensitivity of a mutant V2 receptor suggests a novel therapeutic strategy for nephrogenic diabetes insipidus. *Mol. Endocrinol.* 28, 634–643 (2014).
- C. V. Carman, J.-L. Parent, P. W. Day, A. N. Pronin, P. M. Sternweis, P. B. Wedegaertner,
   A. G. Gilman, J. L. Benovic, T. Kozasa, Selective regulation of Gαq/11 by an RGS domain in the G protein-coupled receptor kinase, GRK2. *J. Biol. Chem.* 274, 34483–34492 (1999).
- L.-F. Seet, W. Hong, Endofin recruits clathrin to early endosomes via TOM1. J. Cell Sci. 118, 575–587 (2005).
- G. Gulyás, G. Radvánszki, R. Matuska, A. Balla, L. Hunyady, T. Balla, P. Várnai, Plasma membrane phosphatidylinositol 4-phosphate and 4,5-bisphosphate determine the distribution and function of K-Ras4B but not H-Ras proteins. J. Biol. Chem. 292, 18862–18877 (2017).
- H. J. Motulsky, L. C. Mahan, The kinetics of competitive radioligand binding predicted by the law of mass action. Mol. Pharmacol. 25, 1–9 (1984).
- C. Stringer, T. Wang, M. Michaelos, M. Pachitariu, Cellpose: A generalist algorithm for cellular segmentation. *Nat. Methods* 18, 100–106 (2021).
- TensorFlow Developers, TensorFlow, version 2.12.0-rc0, Zenodo (2023); https://doi. org/10.5281/zenodo.7641790.
- 87. P. Isola, J.-Y. Zhu, T. Zhou, A. A. Efros, Image-to-image translation with conditional adversarial networks. arXiv:1611.07004 [cs.CV] (2016).
- The pandas development team, pandas-dev/pandas: Pandas, version 1.5.3, Zenodo (2023); https://doi.org/10.5281/zenodo.7549438.
- P. Virtanen, R. Gommers, T. E. Oliphant, M. Haberland, T. Reddy, D. Cournapeau,
   E. Burovski, P. Peterson, W. Weckesser, J. Bright, S. J. van der Walt, M. Brett, J. Wilson,
   K. J. Millman, N. Mayorov, A. R. J. Nelson, E. Jones, R. Kern, E. Larson, C. J. Carey, I. Polat,
   Y. Feng, E. W. Moore, J. VanderPlas, D. Laxalde, J. Perktold, R. Cimrman, I. Henriksen,
   E. A. Quintero, C. R. Harris, A. M. Archibald, A. H. Ribeiro, F. Pedregosa, P. van Mulbregt;
   SciPy 1.0 Contributors, SciPy 1.0: Fundamental algorithms for scientific computing in
   Python. Nat. Methods 17, 261–272 (2020).
- S. Seabold, J. Perktold, "Statsmodels: Econometric and statistical modeling with Python" in Proceedings of the 9th Python in Science Conference (SciPy 2010), pp. 92–96; https:// conference.scipy.org/proceedings/scipy2010/seabold.html.

Acknowledgments: The technical assistance of E. Halász, I. Oláh, and K. Szabolcsi is greatly appreciated. We thank S. S. Ferguson, K. Nakayama, and A. Reményi for providing plasmid constructs. Funding: This work was supported by the Hungarian National Research, Development and Innovation Fund [NVKP\_16-1-2016-0039 (L.H.), NKFI FK 138862 (G.T.), K 139231 (L.H.), and K 134357 (P.V.)] and the Ministry for National Economy [Competitive Central Hungary Operational Programme VEKOP-2.3,2-16-2016-00002 (L.H.)], G.T. was funded by the János Bolyai Research Scholarship and the János Bolyai Research Scholarship Plus of the Hungarian Academy of Sciences BO/00807/21, A.I. was funded by JP21H04791 and JP21H05113 from the Japan Society for the Promotion of Science; JPMJFR215T and JPMJMS2023 from the Japan Science and Technology Agency; and JP22ama121038 and JP22zf0127007 from the Japan Agency for Medical Research and Development. Author contributions: Conceptualization: A.D.T., B.S., G.T., and L.H. Methodology: A.D.T., B.S., A.B., A.I., P.V., and G.T. Investigation: A.D.T., B.S., O.T.K., D.G., S.P., E.S.-K., G.T., and L.H. Visualization: A.D.T., B.S., D.G., and S.P. Funding acquisition: G.T. and L.H. Supervision: G.T. and L.H. Writing: A.D.T., B.S., O.T.K., D.G., S.P., A.B., P.V., G.T., and L.H. Competing interests: B.S. is a current employee of Turbine Ltd. The other authors declare that they have no competing interests. Data and materials availability: All codes applied are openly available at Zenodo (DOI: 10.5281/ zenodo.10072720 and 10.5281/zenodo.10091027). All data needed to evaluate the conclusions in the paper are present in the paper or the Supplementary Materials.

Submitted 3 April 2023 Resubmitted 25 November 2023 Accepted 5 June 2024 Published 25 June 2024 10.1126/scisignal.adi0934